M. TECH. THESIS

on

UNDERSTANDING THE FLOOD-GENERATING MECHANISMS IN A MONSOON-DOMINATED RIVER BASIN

by

SUYASH SHUKLA

DEPARTMENT OF CIVIL ENGINEERING
INDIAN INSTITUTE OF TECHNOLOGY INDORE,
SIMROL, MADHYA PRADESH, INDIA – 453552
MAY 2025

UNDERSTANDING THE FLOOD-GENERATING MECHANISMS IN A MONSOON-DOMINATED RIVER BASIN

A Thesis

Submitted in partial fulfilment of the

requirements for the award of the degree

of

Master of Technology

in

Water, Climate and Sustainability

by

SUYASH SHUKLA

(2302104018)

under the supervision of

DR. PRIYANK J. SHARMA

Assistant Professor, Department of Civil Engineering

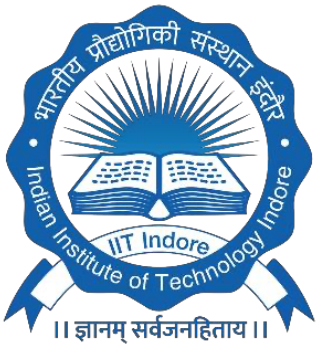

DEPARTMENT OF CIVIL ENGINEERING

INDIAN INSTITUTE OF TECHNOLOGY INDORE,

SIMROL, MADHYA PRADESH, INDIA – 453552

MAY 2025

INDIAN INSTITUTE OF TECHNOLOGY INDORE

CANDIDATE'S DECLARATION

I hereby certify that the work which is being presented in the thesis entitled **Understanding The Flood Generating Mechanisms in a Monsoon Dominated River Basin** in the partial fulfilment of the requirements for the award of the degree of **MASTER OF TECHNOLOGY** and submitted in the **DEPARTMENT OF CIVIL ENGINEERING, Indian Institute of Technology Indore**, is an authentic record of my own work carried out during the time period from May 2024 to May 2025 under the supervision of **Dr. Priyank J. Sharma**, Assistant Professor, Department of Civil Engineering, IIT Indore.

The matter presented in this thesis has not been submitted by me for the award of any other degree of this or any other institute.

Signature of the student with date
(SUYASH SHUKLA)

This is to certify that the above statement made by the candidate is correct to the best of my/our knowledge.

01/06/2025

Signature of the Supervisor of M. Tech. Thesis (with date)
(DR. PRIYANK J. SHARMA)

SUYASH SHUKLA has successfully given his M. Tech. Oral Examination held on **24th May 2025**.

Signature of Supervisor of M. Tech. Thesis
Date: 01/06/2025

Convener, DPGC
Date:

ACKNOWLEDGEMENTS

I would like to express my sincere gratitude to **Dr. Priyank J. Sharma** for his unwavering support and invaluable guidance throughout the course of this project. His mentorship, insightful feedback, and encouragement have been crucial to the progress of my technical report, enabling me to make significant advancements.

I am also thankful to all my **lab mates**, especially **Ms. Achala Singh**, **Mr. Harshvardhan Solanki**, **Mr. Vikas Gore**, and **Mr. Arpit Tiwari** for their exceptional support and collaboration. Their expertise, thoughtful advice, and constructive insights have played a key role in refining my approach and deepening my understanding of essential concepts. The camaraderie and academic exchange within our lab have greatly enriched my research experience.

Furthermore, I would like to express my deepest gratitude to **Dr. Manish Kumar Goyal** (Program Coordinator – WCS), **Dr. Priyansh Singh** (DPGC – Civil Engineering), and **Dr. Abhishek Rajput** (HoD – Civil Engineering) for their unwavering support and guidance. Their dedication to fostering an enriching academic environment has been instrumental in the successful completion of my M. Tech. Thesis.

Lastly, I am profoundly grateful to my **parents** and my **brother** for their constant support, patience, and encouragement throughout this journey. Their belief in me has been a continuous source of strength and motivation.

Date: 24.05.2025 **SUYASH SHUKLA (2302104018)**

ABSTRACT

This study examines changes in flood magnitude and timing across twelve stream gauging stations in the Narmada River Basin from 1972 to 2024. Flood events were identified using the Annual Maximum Series (AMS) and Peaks-Over-Threshold (POT) approaches. Flood frequency analysis employed best-fit probability distributions, with Weibull and Gamma selected for AMS based on the Akaike Information Criterion (AIC). Circular statistics were used to assess flood timing, while magnitudes were categorized into small, moderate, and large floods based on return periods. Notably, large floods were predominantly concentrated in the Sandia catchment under both AMS and POT approaches. Trend analysis using the Modified Mann-Kendall test revealed a significant decline in peak streamflow at most stations, particularly along the mainstem Narmada in the AMS dataset. The POT approach showed a shift toward delayed flood timing at Sandia, Mohgaon, and Garudeshwar. The mean flood timing across the basin typically occurred from early to mid-August. Hydro-meteorological analysis of major flood events indicated that floods were driven by extreme precipitation, catchment wetness, or a combination of both. A catchment-based assessment of sensitivity to antecedent precipitation buildup (APB) revealed that flood magnitudes in upper and upper- mid reaches of catchments were notably correlated with APB. These findings highlight evolving flood dynamics in the Narmada basin and emphasize the need for incorporating catchment-scale processes and antecedent conditions into regional flood management strategies.

Keywords: Flood frequency analysis, Annual Maximum Series, Peaks Over Threshold, Circular Statistics, Trend Analysis, Flood generation mechanisms, Narmada River Basin.

TABLE OF CONTENTS

LIST OF FIGURES

LIST OF TABLES

Chapter - 1

INTRODUCTION

1.1 Background of the Study

Globally, floods present a significant challenge, causing widespread destruction and economic losses. In India, where 80% of annual rainfall occurs during the monsoon season, flooding during this period results in major loss of life and property (NDMA, 2008). Extreme rainfall events, particularly those originating from cyclonic depressions in the Bay of Bengal and the Arabian Sea, drive much of this devastation (Hunt and Fletcher, 2019). The Intergovernmental Panel on Climate Change (IPCC), in its Sixth Assessment Report (IPCC, 2021; Masson-Delmotte et al., 2021), predicts that both extreme and mean precipitation will likely intensify across Asia, especially in South Asia. Despite the overall decline of the southwest monsoon over the Indian subcontinent, Roxy et al. (2015) identified a threefold increase in extreme rainfall events across Central India from 1950 to 2015. With greater climate variability and rising temperatures, flood frequencies and storm runoffs are expected to escalate, which in turn emphasizes the need for understanding trends and mechanisms behind the flood processes.

At a global level, flood studies have provided insights into trends in streamflow and seasonality, including works by Petrow and Merz (2009), Mangini et al. (2018), and Do et al. (2019), who analyzed seasonal flood timings and shifts across various regions. These studies highlight the influence of both climatic changes and catchment characteristics on flood dynamics. Jain et al. (2017) analyzed trends in extreme flood events across prominent river basins in India, highlighting the influence of human activities such as urbanization and reservoir regulation on streamflow patterns. They found that there was either a decrease or no significant trend in flood magnitude at most sites. Similarly, Ganguli et al. (2022) explored trends in streamflow and studied mean flood timing in the Mahanadi River Basin using both annual maximum series (AMS) and peaks-over-threshold (POT) approaches. They found that decreasing trends in flood magnitude are predominant among most stations, while no apparent variations in the mean flooding date was observed using both approaches. Nanditha et al. (2022) investigated the mechanisms underlying flood generation in the Narmada River basin, enhancing the understanding of regional flood processes. They found that most of the rainfall in the basin occurs in July and August. In

contrast, high flows are observed during late August and September, hence emphasizing the importance of antecedent moisture conditions in propagating floods. Thus, understanding the flood generating mechanisms help in improving flood forecasting efforts for effective disaster management operations.

1.2 Motivation and Importance of the Study

Given the increasing incidence of extreme rainfall and flooding, there is a pressing need for localized and robust analysis of flood behavior in vulnerable river basins. Several studies, including those by Rajaguru et al. (1995), Kale et al. (1997), and Kathal (2018), emphasize that the Narmada River basin in central India is not only highly vulnerable to flooding but also one of the most flood-prone regions in the country. The historical records document several major flood events from the early 19th century. The highest recorded discharge of 69,400 cumecs occurred in 1970 at Garudeshwar (Kale et al., 2003). The recent severe flood years include 1973, 1984, 1990, 1994, 2013, 2020, and 2023, with 1994 marking the most intense flooding year amongst these records (Mangukiya et al., 2022). The river's passage through narrow gorges, combined with stable alluvium banks, often leads to increased depth during floods. These geological conditions, along with relatively high rainfall, contribute to the basin's high flash flood magnitude index, making it susceptible to floods (Kale et al., 2002).

In Madhya Pradesh, twenty-one districts fall within the Narmada Basin. According to a study by Pathak et al. (2021), approximately 76% of these districts are categorized as highly flood prone. In addition, the Bharuch and Narmada districts of Gujarat that fall within the Narmada River basin are also prone to recurrent floods (Bhargav et al., 2025). The Narmada basin is predominantly covered by agricultural lands (56.90%), followed by forested areas (32.88%), wastelands (6.13%), and built-up zones (around 3%). Between 2013 and 2019, approximately 8% of the cultivated area in the region was affected by floods. During August and September of 2019, intense rainfall led to the flooding of nearly two hundred villages (Pathak et al., 2021). In 2020, continuous heavy rains caused severe flooding, prompting the National and State Disaster Response Forces to evacuate approximately twenty-five thousand people. The financial impact of the 2020 floods was estimated at around forty-eight million US dollars (SDMA, 2020). The most recent flooding in the basin occurred in 2023, when the Highest Flood Level (HFL) was breached at 13 flood stations - 8 on the main river and 5 on its tributaries (see Table 1.1).

Table 1.1 Flood severity in the Narmada River basin during the September 2023 event (SANDRP, 2023)

Site/River	District	Old HFL (m)	New HFL (m)
Abna at Khandwa/Narmada	Khandwa	301.27	302.95
Hathed at Misrod/Narmada	Hoshangabad	297.35	297.80
Kalimachak at Charuwa/Narmada	Harda	286.20	287.00
Datuni at Dudwas/Narmada	Dewas	252.06	252.16
Kaner at Mendhikheda/Narmada	Khargone	214.81	217.70
Charol at Barwah/Narmada	Khargone	173.90	175.40
Karam at Dahiwar/Narmada	Dhar	166.93	169.66
Mandleshwar/Narmada	Khargone	157.29	158.40
Bhamgarh/Chota Tawa	Khandwa	270.68	275.25
Beda at Satwadi (Gogawa)/Beda	Khargone	205.52	205.70
Maan at Gopalpura/Man	Dhar	195.90	196.30
Deb at Khajuri/Deb	Barwani	180.10	181.38
Barod at Thikri/Barod	Barwani	165.55	168.33

Note: HFL denotes high flood level.

The severity of this event is evident from the displacement of around 9,500 people and the impact on several road and railway bridges. The hydrometeorological conditions leading to flooding in the Narmada Basin are multifaceted. Factors such as the Indian Ocean Dipole (IOD), and Atlantic Multidecadal Oscillation (AMO), and El Niño–Southern Oscillation (ENSO) have been identified as significant contributors to the variability in hydroclimatic extremes (Singh et al., 2023). Additionally, the construction of major reservoirs like Indira Sagar and Sardar Sarovar has influenced flood dynamics (Prajapati et al., 2025). Given these complexities, understanding the trends in flood magnitude and timing, as well as the underlying hydrometeorological drivers, is crucial for effective flood management in the basin.

1.3 Objectives of the study

The present study aims to accomplish the following objectives:

a) To identify the flood seasonality, using circular statistics, derived from annual maximum series (AMS) and peaks-over-threshold (POT) approaches.
b) To analyze the trends in flood magnitude and timing, considering AMS and POT approaches.
c) To estimate the flood magnitude for various return levels and characterize the flood behavior using AMS and POT approaches.
d) To understand the prominent flood-generating mechanisms in the Narmada River basin by analyzing the most severe historical floods.

1.4 Organization of the thesis

Chapter 1 covers the Introduction section, which has four sub-sections, with the first sub-section covering the background of the study, the second sub-section covering the motivation of the study, the third sub-section covering the objective of the study, and finally, the last section covering the organization of the thesis.

Chapter 2 presents the literature review and methodological framework. It begins with a general introduction (Section 2.1), followed by a review of relevant literature (Section 2.2), identification of key research gaps (Section 2.3), and a detailed description of the methods and methodology adopted (Section 2.4). The chapter concludes with a summary (Section 2.5).

Chapter 3 describes the study area. It starts with a general overview (Section 3.1), defines the case study domain (Section 3.2), and discusses streamflow attributes and data length (Section 3.3). The chapter also covers the datasets used (Section 3.4), summarizes major historical floods in the Narmada River basin (Section 3.5), and ends with a concluding section (Section 3.6).

Chapter 4 presents the results and discussion. After an introductory section (Section 4.1), it analyzes the timing of peak floods (Section 4.2), flood frequency and its characterization (Section 4.3), and trends in flood magnitude and timing (Section 4.4). This is followed by a hydro-meteorological analysis of selected flood events (Section 4.5) and a discussion on the role of catchment wetness in flood generation (Section 4.6).

Chapter 5 concludes the thesis by summarizing the key findings (Section 5.1) and outlining the future scope of the study (Section 5.2).

Chapter - 2

LITERATURE REVIEW AND METHODOLOGY

2.1 General

In this chapter, a structured review of relevant literature is presented, covering various aspects of hydrology and flood dynamics in the Narmada River basin. Existing studies have examined the geomorphological characteristics of the basin, the movement and origin of monsoonal storm systems, and the seasonal patterns of flood occurrence. Several works have focused on flood frequency analysis (FFA) and statistical assessments, while others have investigated the underlying mechanisms responsible for generating extreme flood events, including antecedent soil moisture and rainfall intensity. The chapter also outlines the methodological approaches commonly adopted in such studies, including statistical, hydrological, and event-based analyses. Finally, the specific methods employed in this research are detailed, with a focus on identifying dominant flood-generating mechanisms and assessing flood characteristics across the Narmada Basin.

2.2 Literature Review

Kale et al. (1994) highlighted the significant hydrological and geomorphic roles played by high-magnitude monsoonal floods in central India, particularly in the Narmada and Tapi River basins. These floods, recurrent during the monsoon season, are not only among India's most impactful natural disasters in terms of human vulnerability but are also highly effective in driving landscape evolution. Historical, modern, and palaeoflood evidence suggests that such extreme events are frequent and integral to the geomorphic functioning of these river systems. A notable example is the catastrophic flood in the Tapi River during July 1991, triggered by intense rainfall combined with a dam breach, which resulted in one of the highest unit discharges recorded in the region. Flood competence assessments show that the erosive and transport capacities of these rivers during major flood events rival those of the most powerful floods documented globally. The rivers also maintain detailed sedimentological and geomorphic records of palaeofloods, with archives extending over 2,000 years in the Narmada and Tapi basins and up to 5,000 years in the Choral River. Most extreme flood events are linked to synoptic conditions involving Bay of Bengal depressions, indicating a consistent atmospheric control on flood genesis. The study

underscores the limitations of relying solely on instrumental records due to high spatial and temporal flood variability. Consequently, the authors advocate for the integration of geomorphic, sedimentologic, and palaeobotanic evidence into flood hazard assessments and water resource infrastructure planning in India to better capture the true magnitude and variability of flood risks.

Kale and Hire (2004) investigated the geomorphic effectiveness of various flow regimes in the monsoon-dominated and deeply incised Tapi River in central India. The study categorized flows into three types—low, moderate, and large floods—and assessed their geomorphic influence using parameters such as flood magnitude, frequency, stream power, sediment transport, and channel form adjustments. By analyzing multi-date cross-sections and constructing stream power profiles for large floods, the study revealed that the maintenance of the river's bedrock and alluvial channel morphology is primarily governed by infrequent but high-magnitude floods. The incised nature of the channel enhances the effectiveness of large floods by decreasing the width–depth ratio and increasing both flow velocity and energy per unit area. In contrast, low and moderate flows, while more frequent, play a limited role in shaping channel morphology, being primarily responsible for suspended sediment transport. The findings emphasize that suspended sediment load alone is not an adequate measure of geomorphic effectiveness, particularly in monsoonal rivers where channel-shaping processes are dominated by episodic high-energy flood events.

Kale (2008) provides a detailed quantitative assessment of the stream power dynamics and energy expenditure associated with monsoonal floods in the Narmada River over a 51-year period (1949–1999). Using daily discharge data and hydraulic geometry relationships at Garudeshwar, the study estimates daily specific stream power, and the total energy expended during monsoon seasons. The analysis identifies the highest flood event in 1970 with a peak discharge of approximately 69,400 m^3/s. Rivers like Narmada and Tapi flow through narrow gorges, and often during flooding, channels are seldom breached, which results in an increasing depth of inundation during flooding. This underscores the importance of understanding long-term hydro-geomorphic regimes in flood-prone monsoonal basins like the Narmada.

Petrow and Merz (2009) analyzed flood seasonality and magnitude shifts across various basins in Germany. Their study revealed spatial clustering of flooding trends, with significant increases observed in the southern, western, and central regions. Importantly,

these trends were found to be scale-independent, suggesting that climate-driven factors are primarily responsible for the observed changes in flood behavior.

Jain et al. (2017) analyzed trends in extreme flood events and rainfall in India from 1951 to 2001. Their findings showed a decrease in the occurrence of small-magnitude floods but no significant trends in severe floods. Additionally, they observed a decrease in the number of rainy days and an increase in extreme precipitation events. However, these changes were not reflected in streamflow, possibly due to the construction of reservoirs.

Mangini et al. (2018) focused on flood magnitude and frequency trends across Europe. They identified a spatial coherence in the observed trends and found that the AMS series exhibited more pronounced trends in flood magnitude compared to the POT series. Conversely, trends in flood frequency were more evident in the POT series than in the AMS series. This distinction highlights the need for using both approaches for comprehensive flood analysis.

Berghuijs et al. (2019) emphasized the importance of identifying the mechanisms responsible for river flooding to enhance understanding of flood risk dynamics across different timeframes. Their study introduced a novel seasonality-based method to assess the contribution of key flood drivers—namely, snowmelt, high antecedent soil moisture, and extreme precipitation—at a continental scale. Utilizing a comprehensive dataset of annual maximum flow dates from thousands of catchments across Europe (spanning 1960 to 2010), the analysis revealed that annual rainfall extremes were not the dominant cause of most floods. Instead, a significant proportion of flood events resulted from either snowmelt or the overlap of heavy precipitation with already saturated soil conditions. Notably, the contribution of these mechanisms has remained relatively stable over the past five decades. The study underscores the importance of recognizing multiple overlapping flood drivers and provides a valuable framework for future flood hazard assessments and mitigation strategies in a changing climate.

Tarasova et al. (2019) conducted a comprehensive review of classification systems for river floods based on their causative mechanisms, recognizing that flood occurrence, duration, extent, and severity are governed by a multitude of complex processes. The study emphasizes the importance of categorizing flood events by their generating processes to enhance the reliability of flood frequency analysis and to improve the interpretation of long-term changes in flood behaviour. The authors critically evaluated various existing

classification approaches applied to both instrumental and pre-instrumental flood records, noting the absence of a universally accepted framework. Current methodologies typically adopt one of three perspectives: hydroclimatic (focusing on large-scale atmospheric and circulation patterns), hydrological (emphasizing local precipitation and catchment antecedent conditions), and hydrograph-based (inferring causes from flood response characteristics). While each of these approaches contributes valuable insights, the study highlights a significant gap in the systematic evaluation of their robustness, especially regarding uncertainties in input data, indicators, and classification criteria. This limitation reduces the applicability of such methods across diverse geographic regions. The study advocated for more rigorous testing and the incorporation of additional indicators such as spatiotemporal patterns of precipitation, antecedent wetness, and routing effects to develop more reliable and transferable classification frameworks for flood events.

Pathak et al. (2021) introduced a framework based on data envelopment analysis (DEA) for assessing flood vulnerability in river basins, with its application demonstrated through an analysis of twenty one districts within the Narmada River basin in central India. Indicators related to sensitivity and adaptive capacity were selected and integrated to construct a Flood Vulnerability Index (FVI). This technique was applied to examine operational efficiency and the nature of productivity relative to changes in input size, offering valuable insights for informed policymaking and flood risk management. Additionally, districts were grouped according to their vulnerability levels using cluster analysis. The findings indicated that more than three-fourths of the districts exhibited a high degree of flood vulnerability, primarily influenced by socio-economic conditions, geographical size, and the extent of available resources.

Ganguli et al. (2022) examined trends in streamflow and flood timing in the Mahanadi River Basin using both AMS and POT approaches. Their study aimed to identify areas where significant changes in both flood magnitude and timing occurred. Notably, about one-third of the gauging stations showed increasing flood magnitudes alongside delayed flood timings, indicating compounded risks in certain regions.

Nanditha and Mishra (2022) investigated the dominant flood-generating mechanisms in Indian river basins under both current and projected climatic conditions. Recognizing the critical role of non-structural mitigation strategies, such as early warning systems, the study emphasized the need to understand the key drivers of flooding. Through a novel analytical

framework, the study explored the interplay between antecedent moisture and precipitation characteristics preceding high-flow events. The results revealed that multiday precipitation on already saturated soils is the leading cause of floods in both the observed record and future climate scenarios. Their analysis further indicated that in large river basins, sustained heavy rainfall over wet soils plays a more significant role than isolated extreme soil moisture events, whereas in smaller basins, intense short-duration rainfall remains the primary trigger. The study also projected an increase in the frequency of these dominant flood drivers under future warming scenarios, highlighting the growing vulnerability of agricultural areas and infrastructure to hydrological extremes in a changing climate.

Mangukiya et al. (2022) conducted a study focusing on flood risk assessment in the lower Narmada basin, a region historically affected by multiple high-intensity flood events. The study applied statistical flood frequency analysis using Gumbel and Log-Pearson Type III distributions to estimate peak flood discharges for varying return periods. To visualize the extent of flood-prone areas, a hydrodynamic simulation was performed. The study found that the Log-Pearson Type III distribution was more effective in estimating floods for lower return periods, while Gumbel's distribution showed better alignment for higher return periods. The flood inundation modelling revealed that the extent of high-risk flood zones expands with increasing return periods, whereas low-risk areas exhibit minimal change. Based on the findings, the authors concluded that the existing embankments along the Narmada River may not provide sufficient protection during major flood events. The flood hazard maps generated in the study were recommended as decision-support tools for local authorities and planners involved in flood risk management and mitigation efforts.

Nanditha et al. (2022) explored flood generation mechanisms in the Narmada River basin, attributing late August to September high flows to extreme rainfall and heavy precipitation events. They identified the Arabian Sea as the primary moisture source for monsoonal rainfall in the basin. Interestingly, only 60% of extreme precipitation events led to high flood events, whereas 80% of high flood events were preceded by heavy precipitation.

Bari et al. (2023) investigated flood seasonality and timing across Australian gauging stations using circular statistics. They also analyzed trends in flood timing with the Mann-Kendall and the Theil-Sen slope tests. The study concluded that flood peaks in recent years have occured approximately 10–15 days later per decade compared to previous years, indicating a significant delay in flood seasonality.

Fang et al. (2024) investigated changes in flood characteristics across Europe by analyzing spatiotemporally connected flood events using observation-driven routed runoff simulations from the mesoscale Hydrologic Model over the past 70 years. Their study highlights an average 11.3% increase in flood extents across Europe, with notable regional variations. In northern Europe, this increase is driven by higher flood magnitudes due to increased precipitation and snowmelt, while in central Europe, it is attributed to a broader spatial extent of heavy precipitation. The study underscores the utility of combining long-term simulations of runoff along with spatial and temporal flood detection algorithms to identify trends in flood drivers and their charachteristics. These findings emphasize the importance of incorporating changing flood extents into risk assessments, as they present significant challenges for flood control and water resource management.

Fischer et al. (2024) examined the limitations of stationary flood frequency analysis by exploring how long-term climate variability and anthropogenic impacts alter flood-generating mechanisms. Using a robust change-point test based on Gini's mean difference, they detected significant shifts in flood types across Central Europe. Their findings indicate a marked increase in heavy-rainfall-induced floods and a decline in snowmelt-driven floods, particularly a reduction in winter floods, which are increasingly replaced by rainfall-driven events. These changes impact flood quantiles, demonstrating that traditional models, which assume stationary conditions, fail to capture the evolving frequency and drivers of floods. This study emphasizes the importance of non-stationary approaches and type-based flood statistics to adapt flood frequency analysis to changing climatic and hydrological conditions.

Chandel et al. (2025) explored the application of non-stationary flood frequency analysis in the Upper Narmada River basin using the Generalized Additive Models for Location, Scale, and Shape (GAMLSS) framework. This approach was adopted to address the limitations of traditional FFA methods, which assume stationary conditions and rely on predefined probability distributions. The study aimed to enhance flood risk assessment by incorporating non-stationary data and considering relevant covariates such as rainfall, temperature, and land use changes. Hydrological and meteorological datasets were analyzed, with statistical techniques including the Pettitt test for detecting change points and the modified Mann–Kendall test for trend analysis. The results revealed significant temporal shifts in the flood series, along with declining trends at all gauging stations. The performance of various probability distributions within the GAMLSS framework was

evaluated, showing that the log-normal distribution provided the best fit at most locations, while Weibull and Gamma distributions were preferable at others. This study demonstrates the effectiveness of GAMLSS in capturing complex, non-stationary behaviour in flood data and its potential for improving flood risk prediction in evolving hydrological systems.

Parmar and Karmakar (2025) investigated the dominant hydro-meteorological factors responsible for flood generation across central and southern peninsular India, recognizing the evolving nature of flood timing and magnitude under both natural variability and anthropogenic climate change. By employing circular statistical methods, they analyzed 231 watersheds and found that nearly 89% of them are primarily influenced by soil moisture and precipitation excess. Their findings suggest that in larger basins (greater than 70,000 km²), antecedent soil moisture is the key driver of flood events, while in smaller basins (less than 16,000 km²), precipitation exerts a greater influence. Watersheds of similar size produced higher flood magnitudes when dominated by soil moisture, indicating a significant role of antecedent hydrological conditions. Furthermore, topographic wetness index (TWI) exhibited a contrasting influence on flood peaks: it positively impacted flows in soil moisture-dominated basins and negatively in precipitation-driven basins, underscoring the role of surface water retention and runoff dynamics. The study also highlighted that the relative influence of soil moisture diminishes with rising precipitation intensity, indicating a threshold beyond which precipitation becomes the dominant driver. These insights emphasize the importance of integrating key flood-generating descriptors into predictive models and suggest that flood hazard assessments should consider the dominant hydrological processes specific to each watershed, especially under the changing climate regime.

2.3 Research Gap

While several studies have investigated individual aspects of flooding, such as flood frequency analysis (Bhagat, 2017; Pandey et al., 2017; Goel and Ray, 2019; Mangukiya et al., 2022), trends in flood magnitude (Petrow and Merz, 2009; Pandey and Khare, 2018; Waikhom et al., 2023), but there remains a notable lack of comprehensive and integrated flood assessments that bring together multiple flood-generating mechanisms and spatio-temporal trends in flood magnitude and timing. Additionally, although trend analyses on flood magnitudes have been conducted for the Narmada basin, studies specifically addressing trends in flood timing remain scarce or virtually absent. This gap limits our

understanding of temporal shifts in flood occurrence, which is essential for developing effective early warning systems and adaptive flood management strategies. To address these limitations, the present study offers a holistic flood assessment by integrating analysis of trends in flood magnitude and timing, and event-based hydrometeorological characteristics of major floods. Additionally, it provides an in-depth investigation of the various rainfall conditions, such as short-duration intense storms and prolonged multiday precipitation (antecedent precipitation build-up), and the role of catchment wetness leading to catastrophic flooding in the basin. This comprehensive approach aims to improve the understanding of flood-generating mechanisms, thereby supporting more effective flood forecasting and risk management in the Narmada River basin.

2.4 Methods and Methodology

The stepwise methodology adopted for our current study is given in Figure 2.1.

2.4.1 Extracting Flood Series

Flood events in rainfed rivers in India are typically characterized by the maximum streamflow during the southwest monsoon (i.e., June to September). Two primary methods for analyzing flood events are the (a) annual maximum series (AMS) and (b) peaks-over-threshold (POT). The AMS series has been widely used in flood analysis but has significant limitations. It captures only the single highest flow event each year, failing to account for subsequent large floods if multiple events occur in the same year. This omission can prevent accurate representation of the flood regime's complexity (Burn et al., 2016). Another drawback of the AMS series is the inclusion of lower flow values during years of reduced annual discharge, which may not necessarily result in floods and could skew the results while analyzing extreme values (Zadeh et al., 2019). In contrast, the POT series provides deeper insights into the statistical properties of flood events. By selecting multiple peak discharge events each year, the POT approach better utilizes available data, allowing for a more comprehensive understanding of the flood regime. However, a key challenge in implementing the POT method is choosing an appropriate threshold for event selection (Burn et al., 2016). We employed an automatic procedure for identifying the POT series using the SFE_IFC (GitHub - Zhang-Qin-0925/SFE_IFC-Toolbox) toolbox (Zhang et al., 2021) available in MATLAB®. This toolbox facilitates the selection of an optimal threshold and the identification of flood events. The POT series is generally assumed to follow a Generalized Pareto Distribution (Cunnane, 1979), with the toolbox automatically

selecting the most appropriate threshold based on a goodness-of-fit test. Additionally, the independence criteria, as recommended by the United States Water Resources Council, are addressed within this procedure. Further details on the methodology can be found in Zhang et al. (2021). From both methods, we extracted the peak flood magnitude and their timing.

2.4.2 Circular Statistics

To analyze the persistence of flood timing, we employed circular (or directional) statistics, a method commonly used to define both the persistence and timing of flood events (Mardia, 1972). This approach has been applied in various hydrological studies to understand flood seasonality and trends (Burn et al., 2016; Cunderlik et al., 2004). By representing individual flood dates as directional variables, we can calculate a directional mean to identify the central tendency of flood timing over the study period. First, each flood date is expressed in Julian date (JD_i) format and then converted into an angular value (λ_i) in radians using the expression (Laaha and Blöschl, 2006) given below:

$$\lambda_i = JD_i \frac{2\pi}{l(yr)} \tag{2.1}$$

where, i shows peak discharge events, JD_i and q_i indicates the ith Julian day and the discharge corresponding to that day, respectively; $l(yr)$ denotes the number of days in a calendar/water year. For n number of floods, we can calculate the mean event angle ($\bar{\lambda}$) from these equations:

$$\bar{x} = \frac{\sum_{i=1}^{n} q_i \cos \lambda_i}{\sum_{i=1}^{n} q_i}; \bar{y} = \frac{\sum_{i=1}^{n} q_i \sin \lambda_i}{\sum_{i=1}^{n} q_i} \tag{2.2}$$

$$\bar{\lambda} = \begin{cases} \tan^{-1}\left(\frac{\bar{y}}{\bar{x}}\right), & \text{if } \bar{x} > 0 \text{ and } \bar{y} > 0 \\ 180 - \tan^{-1}\left(\frac{\bar{y}}{\bar{x}}\right), & \text{if } \bar{x} < 0 \text{ and } \bar{y} > 0 \\ 180 + \tan^{-1}\left(\frac{\bar{y}}{\bar{y}}\right), & \text{if } \bar{x} < 0 \text{ and } \bar{y} < 0 \\ 360 - \tan^{-1}\left(\frac{y}{x}\right), & \text{if } \bar{x} > 0 \text{ and } \bar{y} < 0 \end{cases} \tag{2.3}$$

The mean flooding date (δ) then can be determined by:

$$\delta = \bar{\lambda} \times \left(\frac{l(yr)}{2\pi}\right) \tag{2.4}$$

2.4.3 Flood Frequency Analysis and Flood Categorization

In this section, we performed flood frequency analysis across all gauging stations in the Narmada River basin by identifying the best-fit statistical distribution for each station. The analysis involved fitting multiple distributions to the data and selecting the best model

for the AMS approach using the Akaike Information Criterion (AIC), which balances model complexity with goodness of fit. For this, the fitmethis toolbox (fitmethis - File Exchange - MATLAB Central) was used in MATLAB. Based on the average and median AIC rankings, we found out the best fit distributions for the AMS series. The Generalized Pareto Distribution (GPD) was pre-selected for the POT series (Cunnane, 1979; Mazas, 2019) due to the automatic threshold selection based on goodness-of-fit tests, as described earlier. Once the best-fit models were determined, FFA curves were plotted for every gauging station, and then return periods for the highest flood events were calculated, providing a quantitative measure of flood risk across the basin.

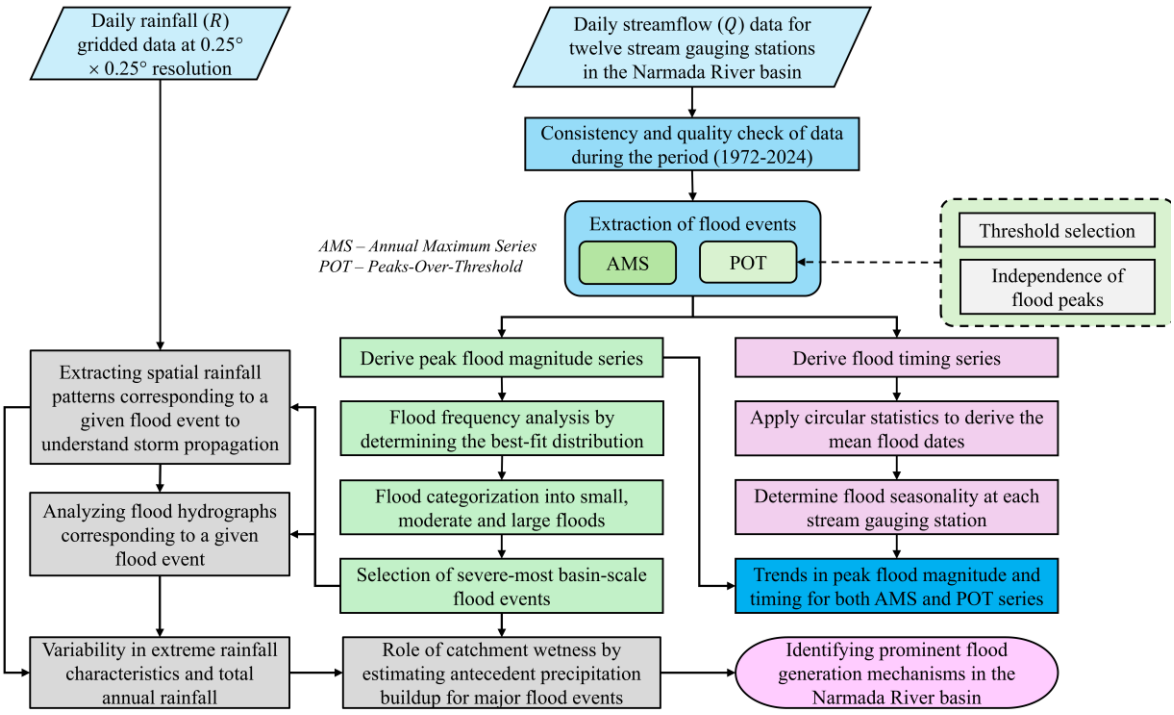

Figure 2.1 Methodology adopted in the present study

Following this, we categorized the flood magnitudes derived from the AMS and POT series into small, moderate, and large floods based on their return periods (T). For the AMS series, the floods with $T_{AMS} \leq 2.33$ years are classified as small floods, $2.33 < T_{AMS} < 6.93$ years as moderate floods, and $T_{AMS} \geq 6.93$ years as large floods, as proposed by Kale and Hire (2004). The return period differs between the AMS and POT models: In the POT model, T_{POT} represents the average interval between the high-flow events that surpass a threshold value Q. T_{AMS} represents the average interval between years that contains a flood

with a flow of at least Q. The relationship between the AMS and POT return periods is defined using the following equation (Langbein, 1949):

$$T_{\mathrm{AMS}} = \left(1 - \exp\left(-\frac{1}{T_{\mathrm{POT}}}\right)\right)^{-1} \tag{2.5}$$

Based on this equation, we established revised thresholds for flood categorization in the POT series. For the POT series, the floods with $T_{POT} \leq 1.78$ years are classified as small floods, $1.78 < T_{POT} < 6.42$ years as moderate floods, and $T_{POT} \geq 6.42$ years as large floods.

2.4.4 Trends in Flood Magnitude and Timing

Trends in flood magnitude and timing are assessed using the non-parametric Modified Mann-Kendall (MMK) test, which is then used for evaluation of trends in both the AMS and POT series. The MMK test is an extension of the traditional Mann-Kendall (MK) test designed to account for autocorrelation within time series data, making it particularly suitable for hydrological studies (Hamed and Rao, 1998). The MMK test is usually implemented for detecting a monotonic trend in a climatological or hydrological time series. The null hypothesis (H_0) states that the time series has no trend, whereas the alternative hypothesis (H_1) describes presence of monotonic trend in the time series. Consider a time series X_t, $t = 1, 2, \ldots, n$, wherein, each data point is systematically compared with all following observations value X_{t+1} forming in a new sequence from which the test statistic S is computed, as originally described by Mann (1945) and Kendall (1975):

$$S = \sum_{k=1}^{n-1} \sum_{j=k+1}^{n} sgn(x_j - x_k) \tag{2.6}$$

where, $sgn(x) = 0$ if $x = 0$, $= -1$ if $x < 0$, and $= +1$ if $x > 0$. The test statistic S can be assumed to follow an approximately normal distribution when $n \geq 18$. Unser this condition, its mean and variance are defined as follows:

$$E(S) = 0 \qquad \text{and}$$

$$Var(S) = \frac{n(n-1)(2n+5) - \sum_{i=1}^{m} t_i(t_i - 1)(2t_i + 5)}{18} \tag{2.7}$$

where, n and m are the number of data and ties, respectively. Each tie represents a set of similar subsequent data in a time series and the data count in each of them is t. The test statistic Z, is computed as:

$$Z = \begin{cases} \dfrac{S-1}{\sqrt{Var(S)}} & ,if\ S > 0 \\ 0 & ,if\ S = 0 \\ \dfrac{S+1}{\sqrt{Var(S)}} & ,if\ S < 0 \end{cases} \quad (2.8)$$

According to Hamed and Rao (1998), the presence of serial correlation in a time series does not affect the limiting normal distribution of the MK test statistic S, nor its expected value. However, it does alter the variance. To account for this, they proposed correction factors that adjust the variance of S by considering only the uncorrelated portion of the series. Positive serial correlation leads to an increase in the variance, while negative correlation causes a decrease. Consequently, a modified approach—referred to as the Modified Mann-Kendall (MMK) test—was introduced. The modified variance $Var(S)*$ for computing the MMK test statistic (Z) is given by:

$$Var\ (S)_* = CF \times Var\ (S) \quad (2.9)$$

where *CF* is the correction factor, which is given as:

$$CF = 1 + \frac{2}{n(n-1)(n-2)} \sum_{k=1}^{n-1} (n-k)\ (n-k-1) \times (n-k-2) r_k^R \quad (2.10)$$

where, r_k^R = ranks of data, and *n* = total length of the time series.

Table 2.1 Classification of trends based on MMK test statistic

MMK Z values	Trend nature
$Z \leq -1.96$	Significant Decreasing (SD)
$Z \geq 1.96$	Significant Increasing (SI)
$Z = 0$	No Trend (NT)
$-1.96 < Z < 0$	Decreasing Trend (D)
$0 < Z < 1.96$	Increasing Trend (I)

The null hypothesis of this test is rejected if the value of $|Z| \geq 1.96$ at a 5% significance level. If the value of Z is positive (negative), it would indicate the presence of an increasing (decreasing) trend in the time series. In this study, a significance level of 5% ($\alpha = 0.05$) is used to determine critical values for hypothesis testing. For a two-tailed test, this resulted in critical Z scores of approximately ±1.96. The Z scores are calculated for each station

based on the MMK test to ascertain whether the null hypothesis of no trend is accepted or rejected. The following thresholds are applied to define trends in flood magnitude based on the calculated Z scores (see Table 2.1).

2.4.5 Event-based Hydro-meteorological Analysis

In this analysis, some of the highest flood events in the Narmada basin, were identified based on the flood categorization. We carefully selected the flood events that occurred before and after the commissioning of Indira Sagar dam, which is the largest dam in the basin. For each event, we determined the peak flood timing (t) and analyzed rainfall patterns leading up to the flood. Using the areal average rainfall, we generated spatial rainfall maps for the basin, applying inverse distance weighted (IDW) interpolation in MATLAB for the period $(t-2)$ to $(t+1)$. IDW estimates rainfall at an unknown location using a weighted average of nearby observations, given by:

$$Z(x) = \frac{\sum_{i=1}^{n} w_i Z_i}{\sum_{i=1}^{n} w_i} \tag{2.11}$$

where, $Z(x)$ is the interpolated value at location x, Z_i represents known values at neighboring points, and w_i is the weight assigned to each point, calculated as:

$$w_i = \frac{1}{d_i^p} \tag{2.12}$$

where, d_i is the distance between the known point and the interpolation location, and p is the power parameter that controls the influence of distant points. In our analysis, we have taken $p = 2$. Additionally, we plotted hydrographs for stations experiencing peak flood conditions to examine the relationship between rainfall intensity and resulting streamflow.

2.4.6 Role of Antecedent Precipitation Buildup (APB)

In this analysis, the top forty POT flood events were selected for each catchment and their dates of occurrence were identified. For each event, we computed the Antecedent Precipitation Buildup (APB) by summing daily precipitation over a 30-day window preceding the peak timing event (t). For a given lag k, APB was defined as the cumulative precipitation from the k-th lag day (relative to the event date) to the 30th lag day:

$$\mathrm{APB}_k = \sum_{i=k}^{30} P_i \tag{2.13}$$

where, P_i is the precipitation on the i-th lag day. Here, k ranges from 0 to 30, with $k = 0$ representing the day of the flood event and $k = 30$ the 30th day prior. To examine the role of antecedent rainfall in flood generation, Spearman's rank correlation was used to assess

the relationship between streamflow and APB for each lag k, based on the top forty POT flood events in each catchment.

2.4.7 Spearman's rho Correlation

Spearman's rho, as introduced by Lehmann (1975), is a non-parametric statistic designed to measure the strength and direction of a monotonic relationship between two variables by working with their ranked data rather than their raw values. This method relies on the assumption that the observations are independent and identically distributed. The test evaluates the null hypothesis (H_0) that no trend exists over time, against the alternative hypothesis (H_1) which asserts the presence of a monotonic increasing or decreasing trend. The test statistic $r_{SR}$and standardized statistic $t_s$are defined as:

$$r_{SR} = 1 - \frac{6\sum_{i=1}^{n}(D_i - i)^2}{n(n^2-1)} \tag{2.14}$$

$$t_s = r_{SR}\sqrt{\frac{n-2}{1-r_{SR}^2}} \tag{2.15}$$

In the context of these equations, D_i refers to the rank corresponding to the i^{th} data point, where i denotes its position in chronological order, and n represents the total number of observations within the time series. The test statistic t_s is evaluated using the Student's t-distribution with $n-2$ degrees of freedom. A positive value of t_s suggests a rising trend over time, while a negative value implies a downward trend. To determine statistical significance at the 5% level ($\alpha = 0.05$), the calculated value of $|t_s|$ is compared against the critical value $t_{(n-2,1-\alpha/2)}$. If this condition is met, the null hypothesis (H_0)-which assumes no trend-is rejected, indicating that the time series exhibits a meaningful trend.

2.5 Closure

This literature review highlights key findings from past studies and identifies gaps in the comprehensive understanding of flood-generating mechanisms across the basin. Building on this foundation, the subsequent sections describe the methodology adopted in this research to address these gaps and provide a detailed analysis of flood dynamics in the Narmada River basin. This approach aims to contribute valuable insights for improved flood hazard assessment and management in the region.

Chapter - 3

STUDY AREA

3.1. General

This chapter provides an overview of the Narmada River basin, the focus area of this study. It begins with a general description of the basin's geographic, climatic, and hydrological characteristics that influence its flood regime. The chapter then details the selection of hydrological stations used for streamflow analysis, including their locations and significance within the basin. Following this, the sources and nature of the streamflow and rainfall data sets utilized in the study are described, emphasizing data quality and temporal coverage. Finally, a historical account of major flood events in the Narmada basin is presented, summarizing the chronology and impacts of significant floods that have shaped the region's flood hazard profile.

3.2. Case Study Domain

The Narmada River basin (see Figure 3.1) encompasses an area of 98796 km² (Subramanya and Sharma, 2024). The name "Narmada" is derived from Sanskrit, signifying the *harbinger of joy*, and it represents one of central India's most prominent rivers. The river originates in the Amarkantak hills of Madhya Pradesh and flows westward into the Gulf of Khambhat in the Arabian Sea. As the largest west-flowing river in India, the Narmada River is often referred to as the lifeline of Madhya Pradesh and Gujarat. The basin encompasses the steep northern slopes of the Satpura Range and the southern slopes of the Vindhya Range. It is fed by forty-one tributaries that converge into the main river from these ranges (Jain et al., 2007). The basin has an elongated shape, extending 234 km from north to south and 953 km from east to west. The eastern region of the basin receives more rainfall, which progressively decreases toward the west, with the basin's average annual rainfall amounting to 1120 mm (Nandhita et al., 2022). The river passes constantly through restrained rocky gorges and rapids before expanding into meandering alluvial reaches (Rajaguru et al., 1995a, b). Stretching approximately 1312 km in length, the Narmada is the fourth longest river confined entirely within Indian territory and is recognized as a natural divide between northern and southern India.

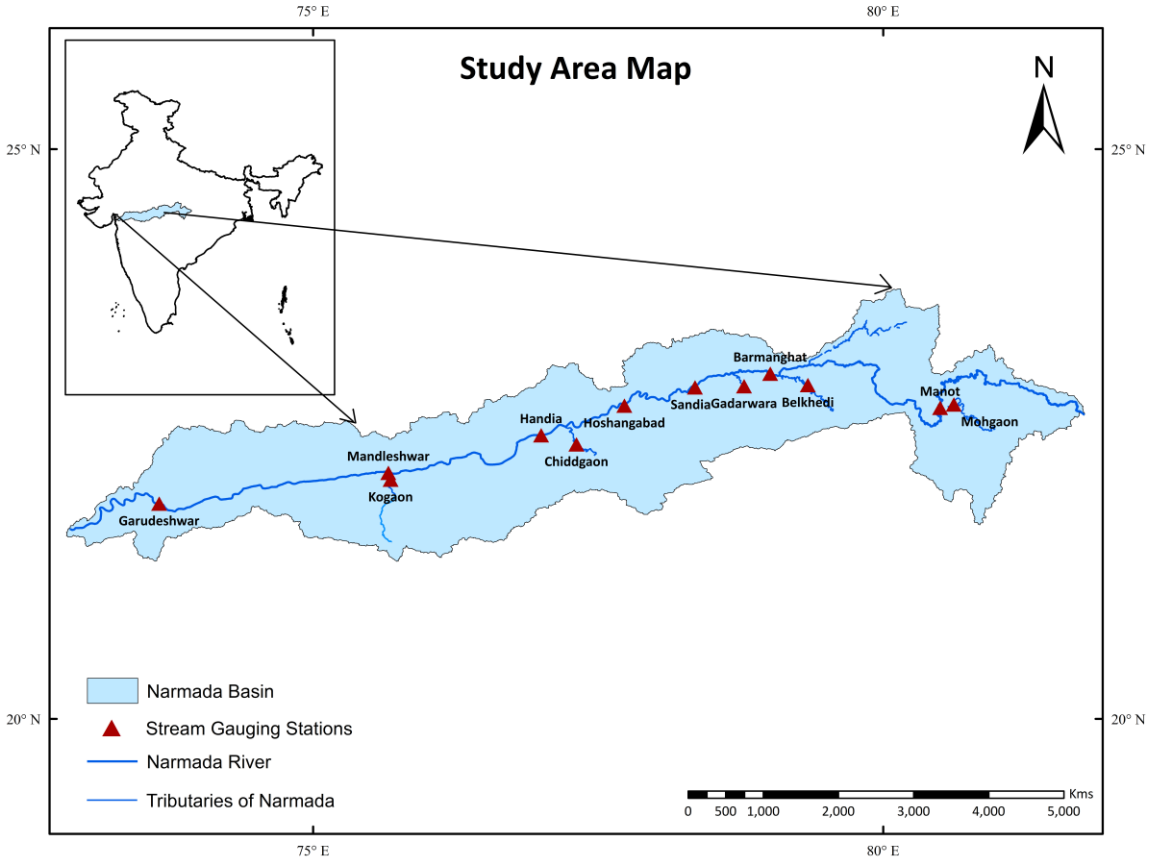

Figure 3.1 Overview of the Narmada River basin, featuring the locations of stream gauging stations.

3.3. Streamflow Data Attributes

For this study, we utilized data from twelve stream gauging stations across the Narmada River Basin, consisting of seven stations located along the main river and five situated on its tributaries. The dataset length and the geographical details of these stations are provided in Table 3.1. Daily streamflow data used in this study were obtained from the India-WRIS web portal (https://indiawris.gov.in/wris/#/RiverMonitoring) and the Bhopal and Surat offices of the Central Water Commission (CWC), India. The dataset comprises measurements from twelve stream gauging stations located within the Narmada River basin. Only stations with continuous data availability for over thirty years were considered for analysis, ensuring long-term reliability. All data underwent rigorous quality control procedures. The streamflow records were reformatted into a water year cycle, defined from June 1st to May 31st. Missing values, limited to a maximum of two consecutive days, were interpolated using a moving average method to maintain data continuity. The gridded rainfall data were sourced from the India Meteorological Department (IMD), Pune

(https://imdpune.gov.in/), at a spatial resolution of 0.25° × 0.25°. The dataset, available in gridded format, was extracted and subset for the Narmada River basin to support hydro-meteorological analysis.

Table 3.1 Attributes of the stream gauging stations analyzed in the study

Stream gauging station	River/ Stream	Latitude (°N)	Longitude (°E)	Data length	
				Start year	End year
Barmanghat	Narmada	23.03	79.01	1972	2024
Belkhedi	Sher	23.12	79.40	1977	2024
Chhidgaon	Ganjal	22.33	76.97	1978	2024
Gadarwara	Shakkar	22.92	78.78	1977	2024
Garudeshwar	Narmada	21.89	73.65	1978	2023
Handia	Narmada	22.49	77.00	1977	2024
Hoshangabad	Narmada	22.75	77.73	1973	2024
Kogaon	Kundi	22.25	76.00	1978	2024
Mandleshwar	Narmada	22.16	75.66	1972	2024
Manot	Narmada	22.73	80.50	1978	2024
Mohgaon	Burhner	22.76	80.63	1978	2024
Sandia	Narmada	22.91	78.35	1978	2024

3.4 Historical Floods in Narmada

The Narmada basin has a long history of major floods, with evidence dating back 5,000 years in the Choral River (Kale et al., 2003). Most floods were caused by Bay of Bengal depressions. The basin is heavily monsoon dominated, receiving nearly 90% of its annual rainfall between June and October, with about 60% concentrated in July and August alone (Narmada Basin Report, CWC 2014). This strong monsoonal influence governs the basin's hydrology and plays a key role in generating floods and shaping streamflow patterns. Historical records from 1818 to 1984 document several severe events. As shown in the Figure 3.2, flood frequency was especially high between 1950 and 1990. Flood records for the basin can be seen in Table 2.2.

Table 3.2 Major historical floods in Narmada basin during 1818-2023 (Kale et al., 2003)

Period	Flood years
Early Records	1818, 1823, 1832, 1854, 1855, 1868, 1878, 1891, 1893, 1894, 1895, 1898, 1905, 1907, 1923, 1926, 1937, 1944, 1945
Mid-20th Century	1961, 1968, 1970, 1984
Recent Years	1994, 1999, 2006, 2009, 2013, 2016, 2020, 2023

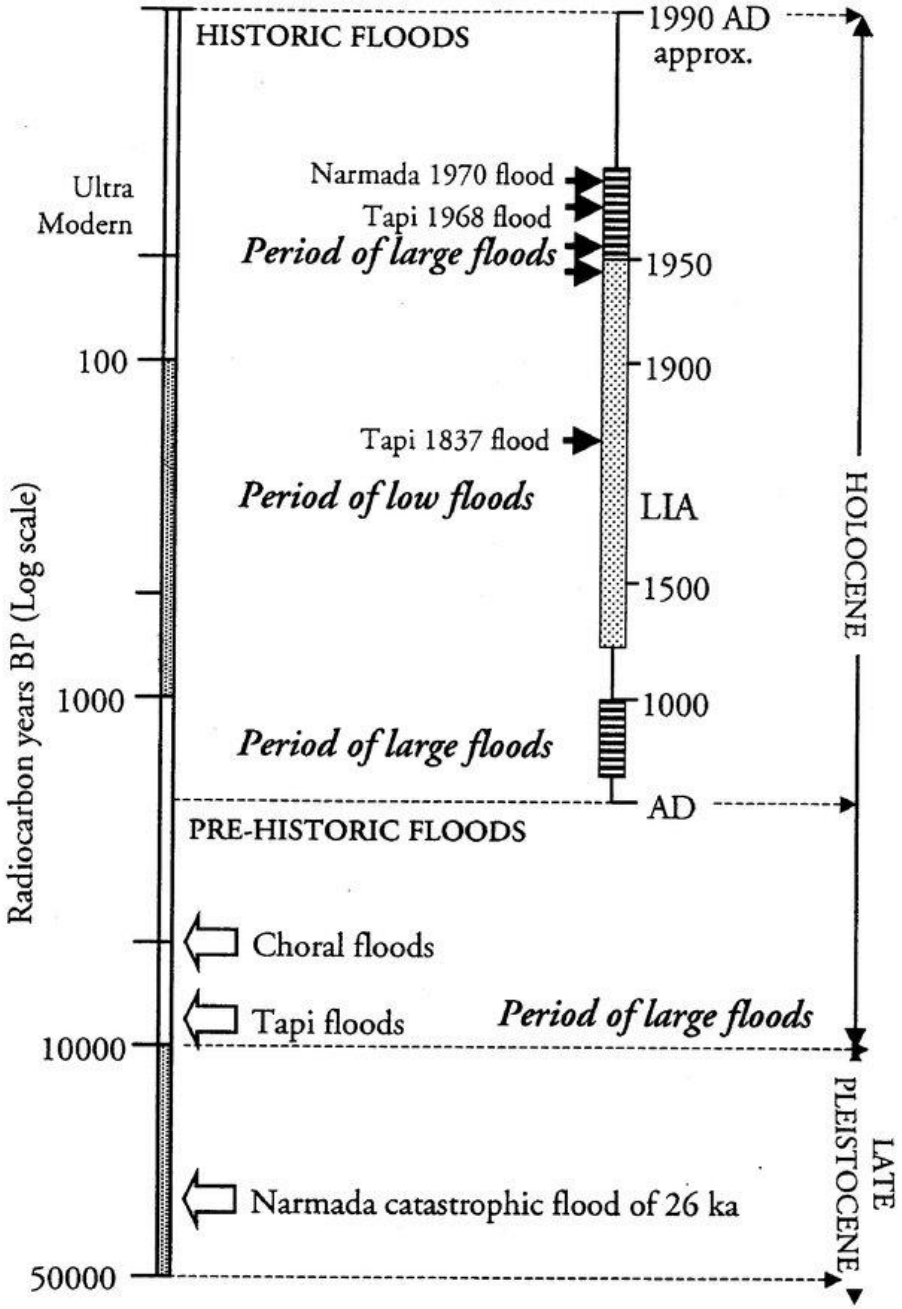

Figure 3.2 Chronology of floods in the Narmada basin (Kale et al., 2003)

3.6 Closure

This chapter provides the essential background and data framework necessary for the analysis that follows. Understanding the basin's physical setting, data availability, and flood history is critical for contextualizing the study results and interpreting the hydrological patterns observed. The detailed description of study sites and data sources lays the groundwork for the subsequent statistical analysis of floods.

Chapter - 4

RESULTS AND DISCUSSIONS

4.1. General

This chapter presents the key findings of the study through a detailed analysis of flood characteristics in the Narmada basin. It begins with an examination of flood seasonality using circular statistics to determine the flood timing at various hydrological stations. Following this, flood frequency analysis is conducted to identify the best-fit statistical distributions and to estimate return periods of observed peak flows. The floods are then classified into small, moderate, and large categories, which enables further investigation into trends in flood magnitude and timing across the basin. The chapter concludes with a hydro-meteorological analysis of selected flood events, employing both event-based and catchment-scale approaches to elucidate the dominant flood-generating mechanisms.

4.2. Timing of Peak Floods

Circular statistics are used to determine the timing of peak floods in the Narmada River basin. Figures 4.1 and 4.2 display the directional statistics of floods using the AMS and POT approaches for stations on the mainstream Narmada and on the tributaries (including Manot), respectively. In Figures 4.1 and 4.2, the periphery of the circle is a measure of the timing of floods, and the radial lines represent flood magnitudes. Using the AMS approach, a total of 585 flood events have been analyzed across all stations. Of these, 2.12% occurred in June, 20.51% in July, 47.69% in August, and 28.38% in September, and 0.68% in October. Similarly, for the POT series, 1231 flood events have been recorded, with 4.22% occurring in June, 21.45% in July, 46.63% in August, 25.35% in September, 2.27% in October, and 0.08% in November. One peculiar thing to notice in these plots is that the highest flood events ever recorded at the stations on the mainstream Narmada River have occurred post-15th August (see Figure 4.1). In contrast, the tributaries exhibit significant variation in their highest recorded flood events, which typically occur between mid-July and late September (see Figure 4.2).

The mean flooding date is then calculated using circular statistics, for all twelve stations (see Table 4.1). In Table 4.1, the range is expressed as the difference between the

latest Julian day and the earliest Julian day of flood occurrences for a given station across all events. The results show that the mean flooding date is mostly observed during early to mid-August across the Narmada basin, with the timing of mean flooding in the tributaries occurring 3-7 days earlier than in the main river. Also, the mean flooding date using both AMS and POT does not exhibit much variation. For all the stations the maximum difference in flood timing for AMS and POT approaches was within a week. Notably the Kogaon station exhibits the widest range in peak flood timing across both AMS and POT approaches, indicating significant variability in peak flood occurrences in the Kundi River. Additionally, tributaries such as Burhner (Mohgaon) and Shakkar (Gadarwara) also demonstrate considerable variations in their peak flood timings.

Table 4.1 Flood timing characteristics derived by using both the AMS and POT approaches

Stream gauging station	Mean flood date (dd/mm)		Days between latest and earliest occurrence of flood event (days)	
	AMS	POT	AMS	POT
Barmanghat	18/08	18/08	81	95
Belkhedi	12/08	11/08	90	99
Chhidgaon	10/08	12/08	78	127
Gadarwara	11/08	11/08	93	99
Garudeshwar	14/08	20/08	101	78
Handia	16/08	14/08	77	108
Hoshangabad	14/08	18/08	75	86
Kogaon	12/08	13/08	113	152
Mandleshwar	21/08	17/08	78	79
Manot	12/08	10/08	85	117
Mohgaon	06/08	12/08	95	114
Sandia	18/08	15/08	78	104

Note: Julian days starting from the beginning of water year (i.e. 1st June).

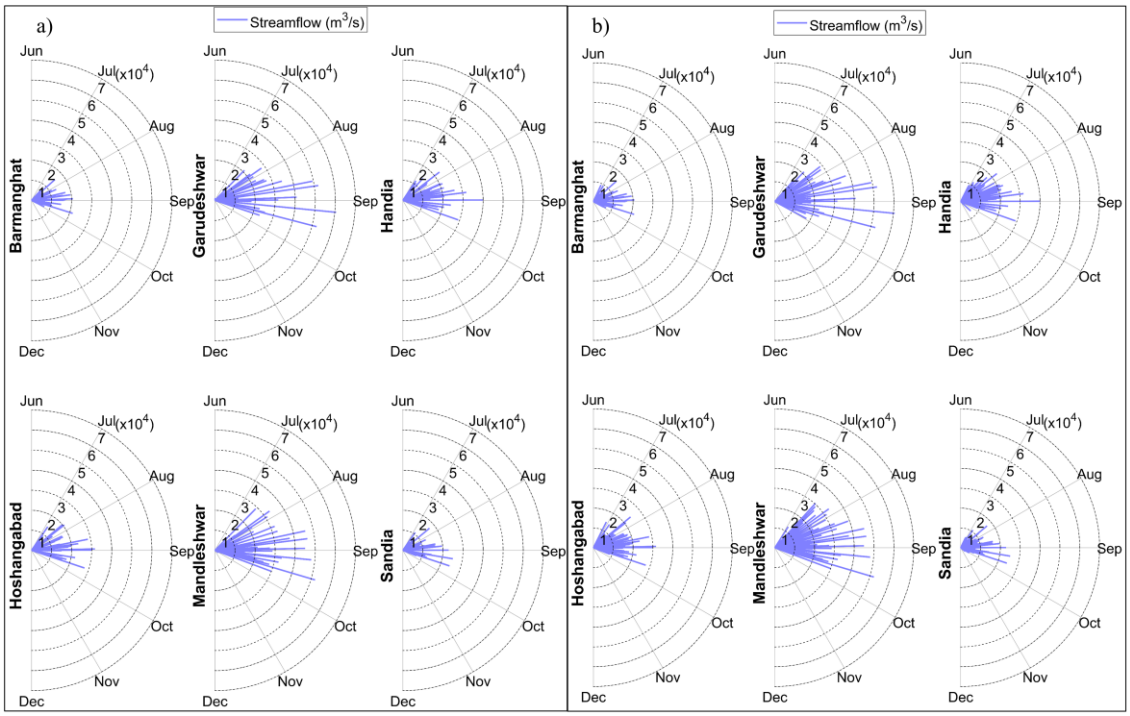

Figure 4.1 Magnitude and direction of peak floods for stations on the mainstream Narmada River basin using (a) AMS and (b) POT approaches.

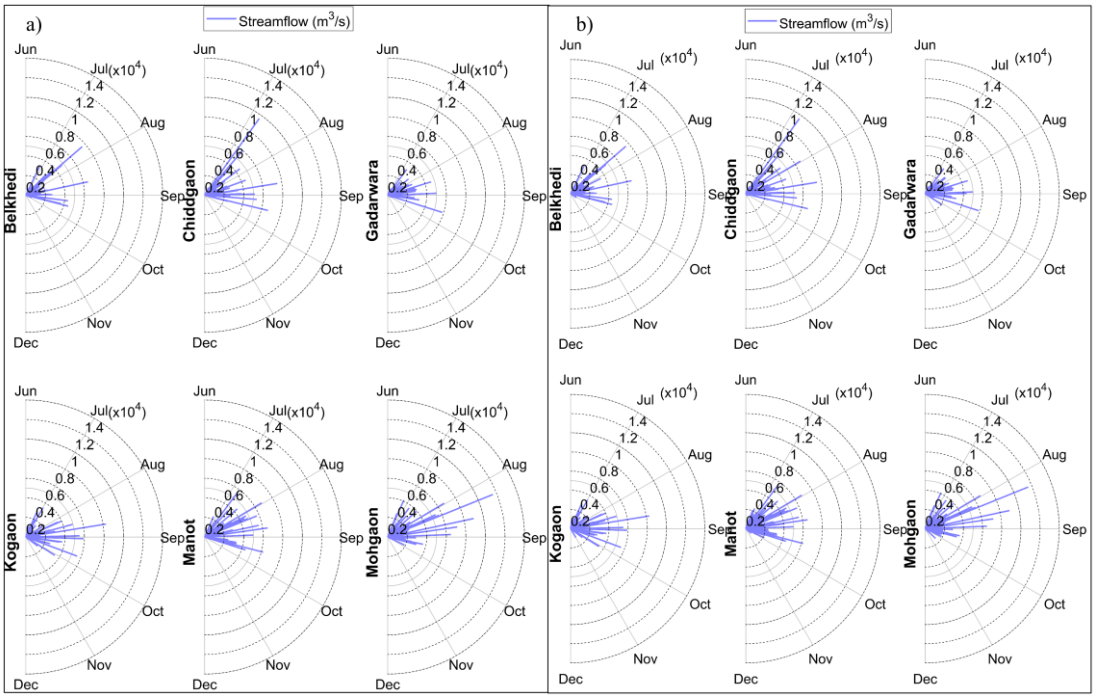

Figure 4.2 Magnitude and direction of peak floods for stations on the tributaries of the Narmada River basin and Manot (on the main Narmada River) using (a) AMS and (b) POT approaches.

4.3. Flood Frequency and Characterization

In this section, we calculated the return periods for all flood events across the twelve gauging stations included in our study. For the AMS series, the Weibull distribution was found to be the best fit for all stations on mainstream Narmada, while Gamma was found to be the best distribution for tributaries and Manot (on Narmada River). Subsequently, the return periods for all flood events are calculated based on these best-fit distributions. The Generalized Pareto Distribution (GPD) was adopted for the POT series. The return period for the highest flood event observed at each station using both the AMS and POT approaches is summarized in Table 4.2. The highest flood was recorded at the Garudeshwar station in 1994, with a peak discharge of 60642 cumecs. The return period corresponding to this flood for the AMS and POT approach was 47 years and 98 years, respectively.

From the fitted distributions, FFA curves are developed for each catchment (see Figure 4.3). For the AMS, FFA curves are plotted using the two best-performing distributions based on AIC values. For the POT method, the GPD was employed, as it was assumed a priori for flood event identification. The POT approach offers a more event-oriented framework for return period estimation, as it focuses on actual flood events that exceed a defined threshold. In contrast, the AMS approach may include relatively low peaks from non-flood years, which can influence distribution fitting and reduce accuracy. Notably, the threshold at each station obtained from the POT analysis were close to the 1.5 to 2-year return period, which typically corresponds to the bankfull discharge (Williams, 1978). This further justifies the selection of threshold values and reinforces the relevance of the POT method in capturing geomorphologically significant flood events. Thus, the POT-based FFA provides a more realistic and hydrologically meaningful characterization of extreme flood behavior across the basin.

Also, as seen in Table 4.2, the return periods estimated for Mohgaon using the AMS series are significantly higher compared to those from the POT series. This difference is explained by the behavior of the FFA curves shown in Figure 4.3, where the AMS Gamma distribution begins to flatten around 9,000 cumecs, indicating that higher return periods yield only small increases in discharge. In contrast, the POT curve does not exhibit the same degree of flattening, resulting in comparatively lower return periods for similar discharge values. A similar pattern is observed for Handia, where the FFA curve begins to flatten around 30,000 cumecs for the POT series and 35,000 cumecs for the Weibull series.

Beyond these points, further increases in return periods correspond to only low-modest increases in discharge.

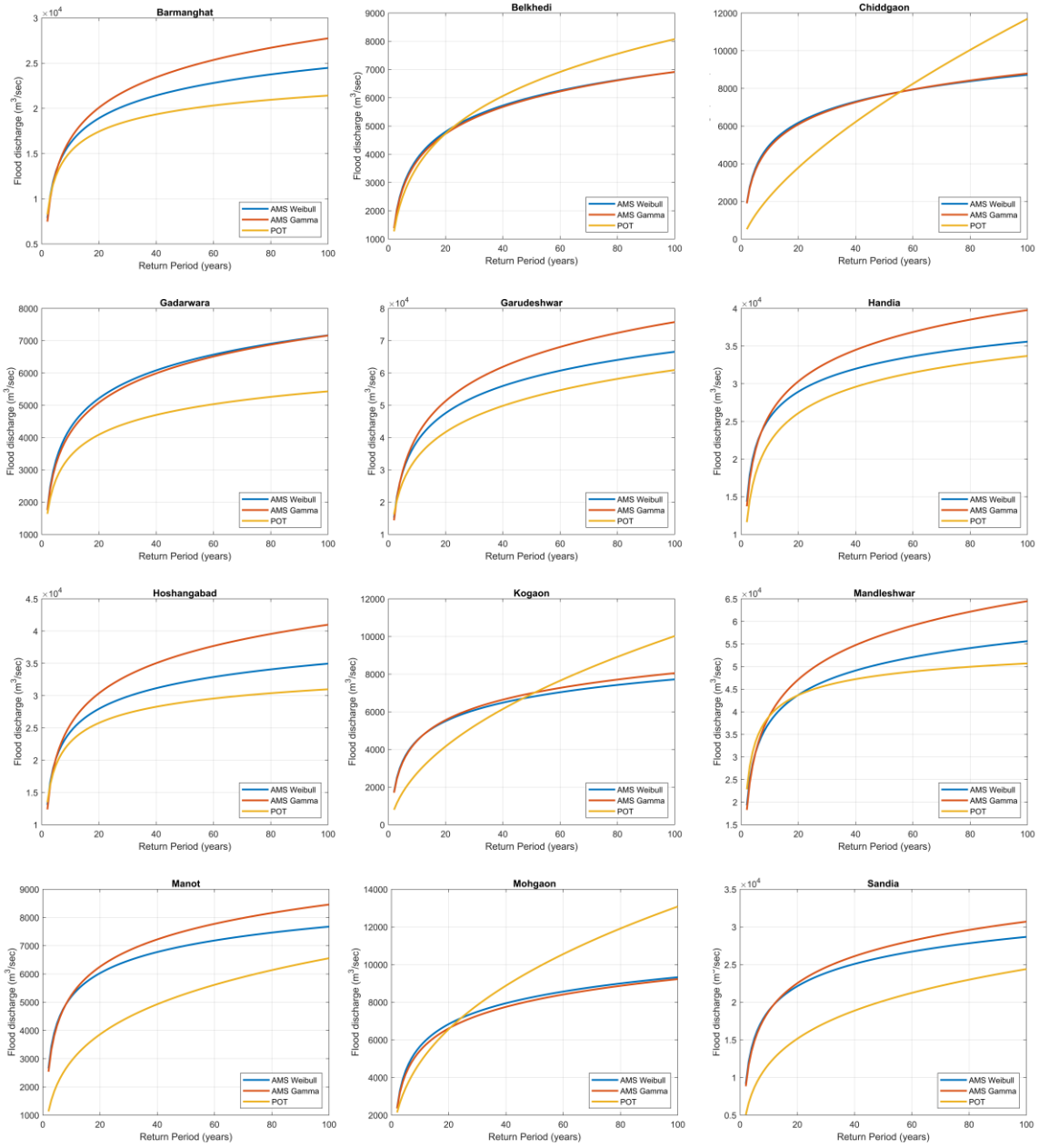

Figure 4.3 Flood Frequency Analysis (FFA) curves for all stream gauging stations considered in this study. *The AMS approach is represented using Weibull and Gamma distributions, while the POT approach employs the Generalized Pareto distribution for threshold exceedances.*

Table 4.2 Return levels of the highest observed flood at each gauging station, estimated using AMS and POT approaches.

Stream gauging station	Highest observed flood event and magnitude		Return period (T) of the highest flood event (years)	
	Year	Q (m^3/s)	AMS	POT
Barmanghat	1999	21500	41	104
Belkhedi	1994	7600	167	82
Chhidgaon	2007	9625	166	75
Gadarwara	1999	5850	89	178
Garudeshwar	1994	60642	47	98
Handia	2020	40000	356	552
Hoshangabad	1973	31600	44	127
Kogaon	1990	8300	118	70
Mandleshwar	2023	52000	44	155
Manot	2006	6806	30	114
Mohgaon	2004	11600	455	75
Sandia	2009	25288	79	115

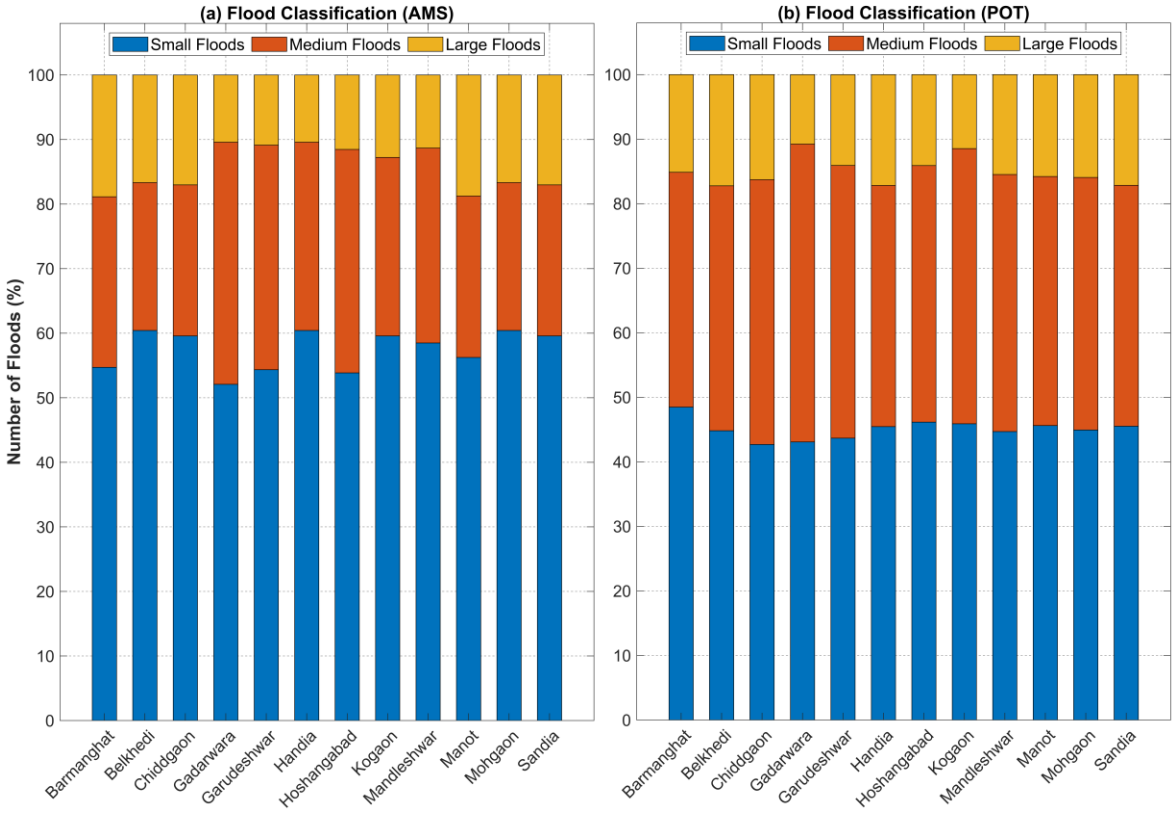

Figure 4.4 Percentage of small, moderate, and large floods at each gauging station, using both the AMS and POT approaches.

Furthermore, we categorized floods into small, moderate, and large based on their return periods as per the criteria listed in Section 2.4.3. Figure 4.4 indicates that the percentage of large floods in the mid-lower reaches of the Narmada River (Hoshangabad, Handia, Mandleshwar, and Garudeshwar) is relatively lower for the AMS-based estimation than the POT. On the contrary, the upper reaches of the basin (Manot, Barmanghat, and Sandia) have a relatively high percentage of large floods based on the AMS approach. This could plausibly be due to the regulating effect of Indira Sagar and Sardar Sarovar dams in attenuating the flood peaks, particularly post year 2006, for Mandleshwar and Garudeshwar. Notably, the percentage of medium flood events is remarkably higher for POT throughout the basin. Also, from both approaches, Sandia has one of the highest percentages of large floods among all stations. Additionally, the POT approach highlights Belkhedi and Handia for large floods.

4.4. Trends in Flood Magnitude and Timing

The trends in flood magnitude and timing are analyzed using the Modified Mann-Kendall (MMK) test for both AMS and POT-extracted flood events (see Figure 4.5). The results highlight distinct differences in trends between the AMS and POT derived floods. For flood magnitudes, the AMS series largely displays decreasing trend, particularly with a significant decline is noted at four mainstream Narmada stations (Barmanghat, Hoshangabad, Mandleshwar, and Garudeshwar) and three along the tributaries (Mohgaon, Belkhedi, and Gadarwara), indicating a reduction in flood intensity in the basin. In contrast, the POT series presents mixed results: Hoshangabad station shows a significant decrease in flood magnitude; Barmanghat, Belkhedi, Chiddgaon, Gadarwara, Mandleshwar, Garudeshwar, Mohgaon and Kogaon stations exhibited decreasing trends, whereas Handia, Sandia, and Manot stations showed increasing trends.

In terms of flood timing (Julian Day), the AMS series does not indicate significant trends, but an increasing trend is noted at most mainstream stations particularly in the mid and lower reaches of the basin. The Mohgaon, Belkhedi, and Chiddgaon stations across the tributaries show decreasing trends, while Kogaon displays an increasing trend. Conversely, the POT series highlights a significant delay in peak floods at Mohgaon, Sandia and Garudeshwar stations, where floods occurrences are delayed in the monsoon. Across other stations, the timing of POT events shows an increasing trend at all stations; except Belkhedi and Gadarwara.

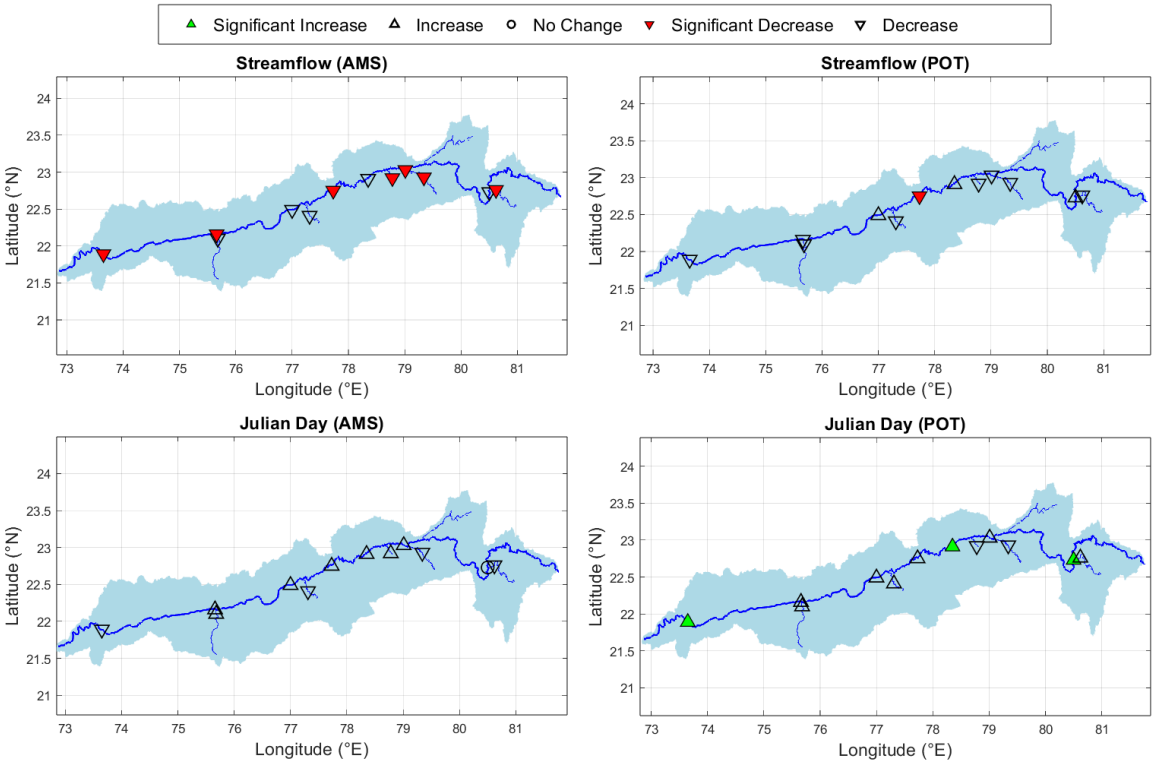

Figure 4.5 Spatial map showing trends in flood magnitude (1-day maximum streamflow) and timing (Julian day of 1-day maximum streamflow) using Modified Mann-Kendall test.

4.5. Hydro-meteorological Analysis of Flood Events

In this section, the top seven flood events (1973, 1984, 1994, 1999, 2013, 2020 and 2023) were selected in the Narmada basin based on flood frequency analysis and its classification. Following this, rainfall variability for a temporal window of four days were plotted—the peak flow (t), two days preceding the peak flow ($t-2,\ t-1$), and one day succeeding the peak flow ($t+1$), along with hydrographs for the corresponding peak flow events. Here, t represents the actual date of peak discharge at given stream gauges. In this analysis the chosen flood events were distinctly clustered into two classes: pre-2006 and post-2006, to delineate the regulation effect of Indira Sagar dam. The pre-2006 flood events include 1973, 1984, 1994, and 1999, while post-2006 flood events were 2013, 2020, and 2023.

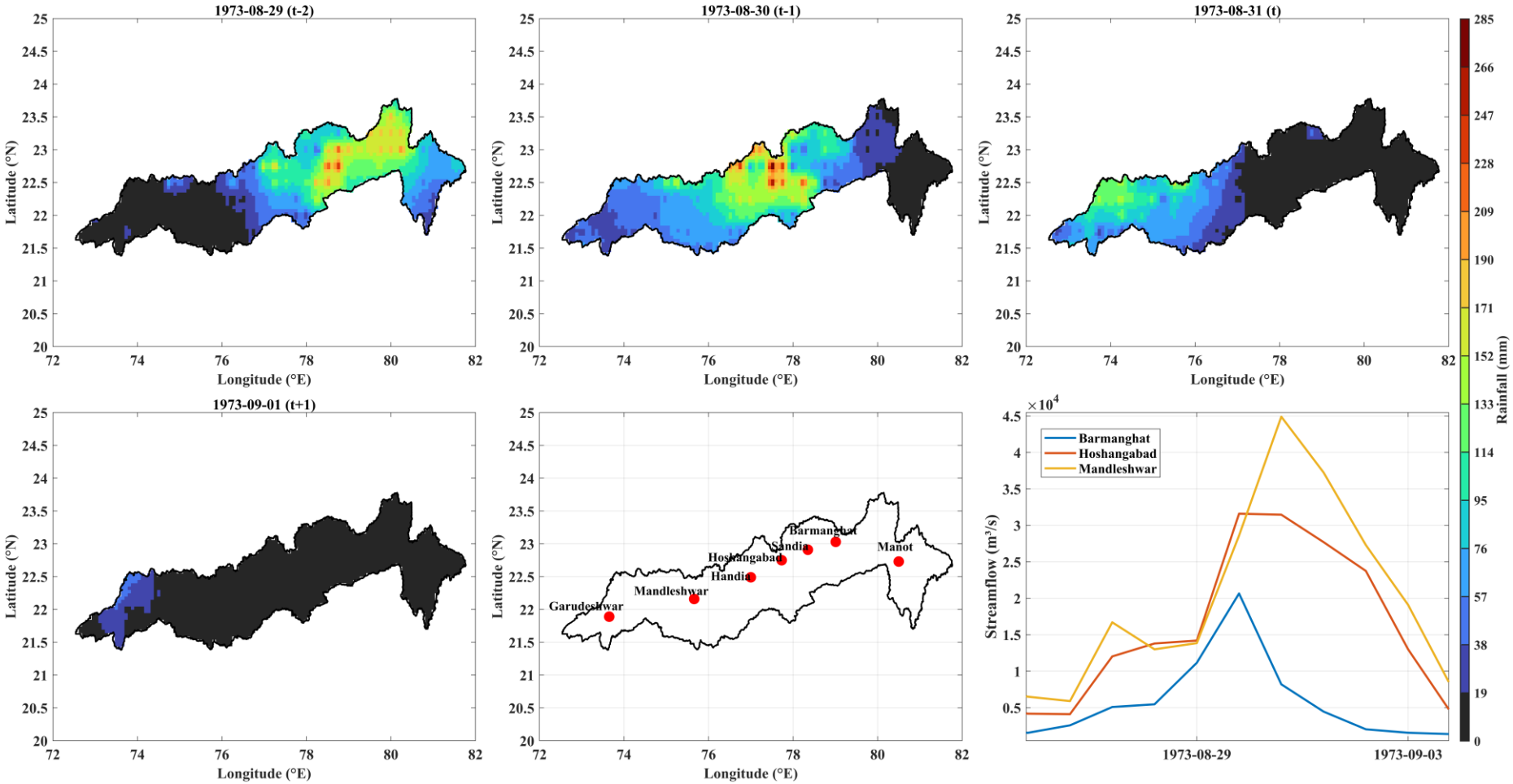

Figure 4.6 Spatial variability of daily rainfall, from day $(t-2)$ to $(t+1)$, across the Narmada River basin for the 1973 flood event and corresponding flood hydrograph for different stream gauges, where t represents the date of the peak flow.

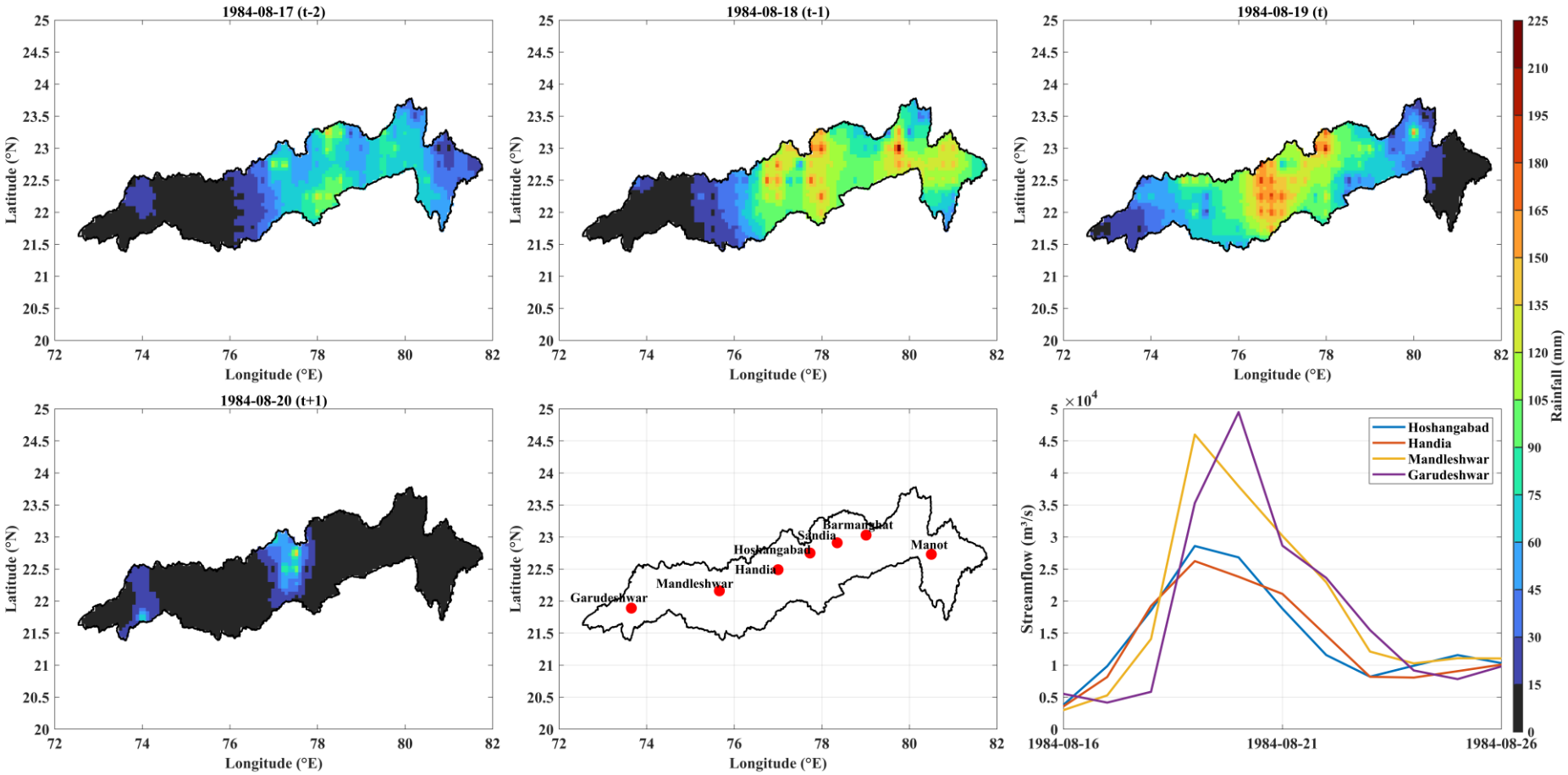

Figure 4.7 Spatial variability of daily rainfall, from day $(t-2)$ to $(t+1)$, across the Narmada River basin for the 1984 flood event and corresponding flood hydrograph for different stream gauges, where t represents the date of the peak flow.

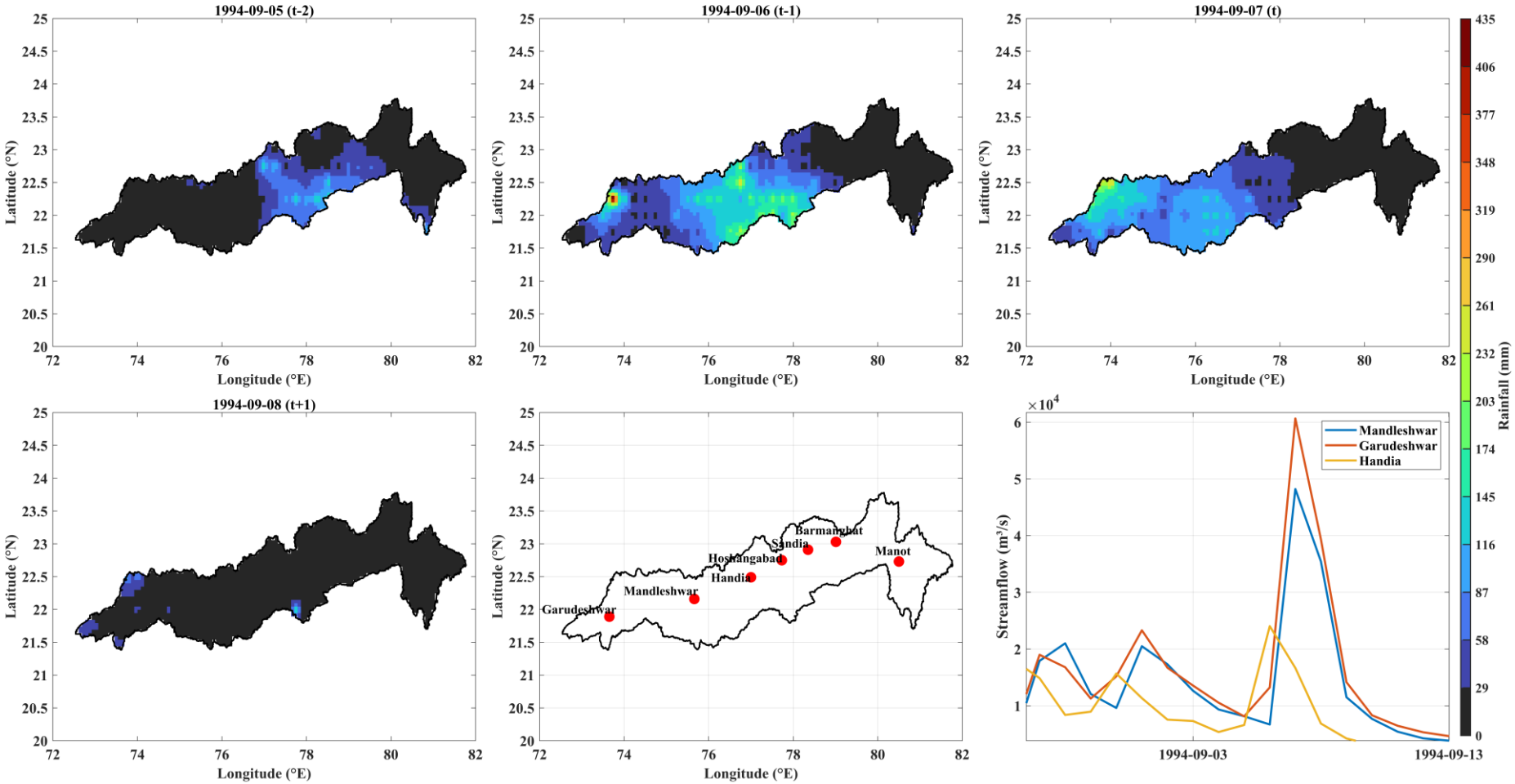

Figure 4.8 Spatial variability of daily rainfall, from day $(t-2)$ to $(t+1)$, across the Narmada River basin for the 1994 flood event and corresponding flood hydrograph for different stream gauges, where t represents the date of the peak flow.

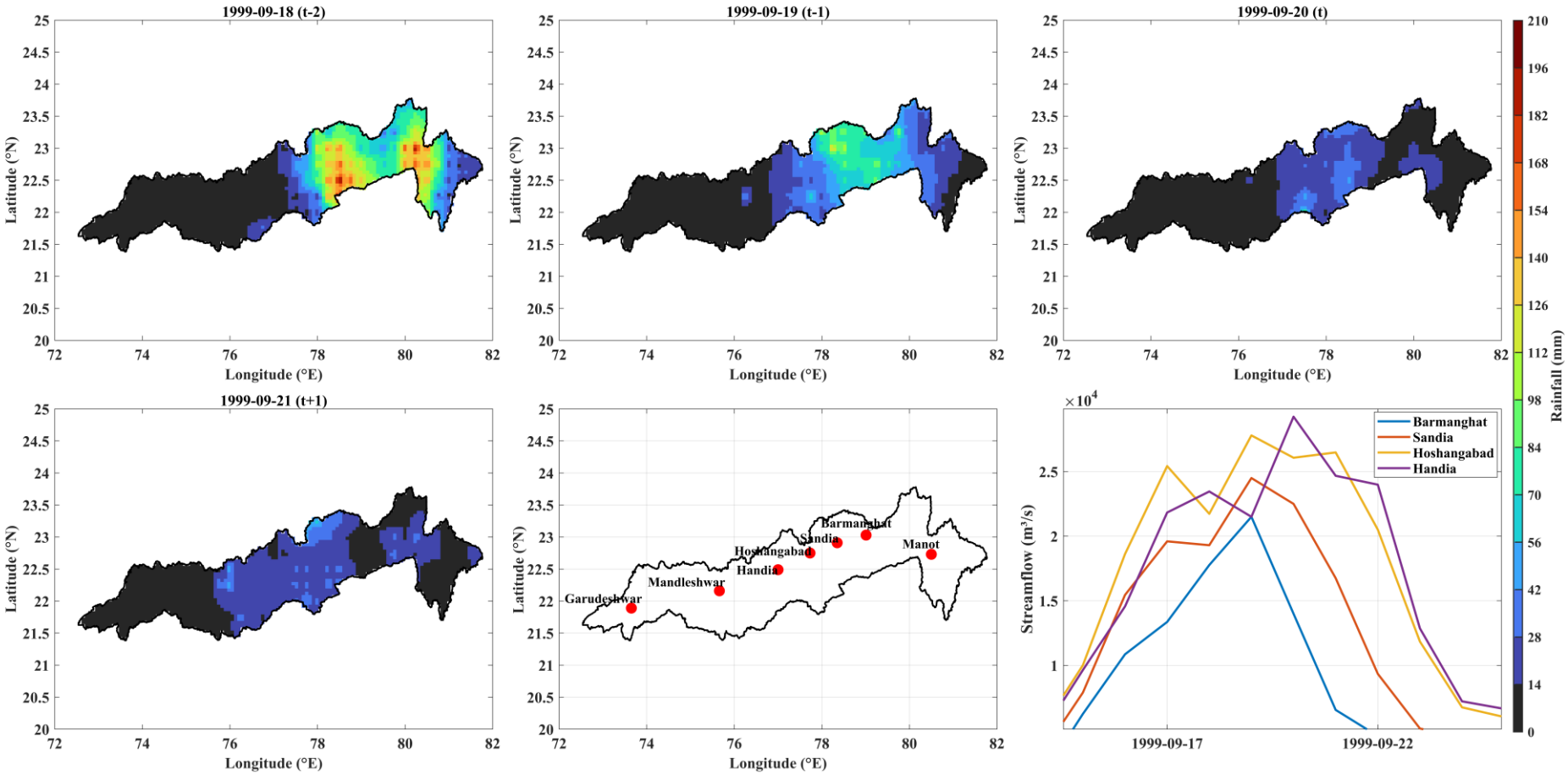

Figure 4.9 Spatial variability of daily rainfall, from day $(t-2)$ to $(t+1)$, across the Narmada River basin for the 1999 flood event and corresponding flood hydrograph for different stream gauges, where t represents the date of the peak flow.

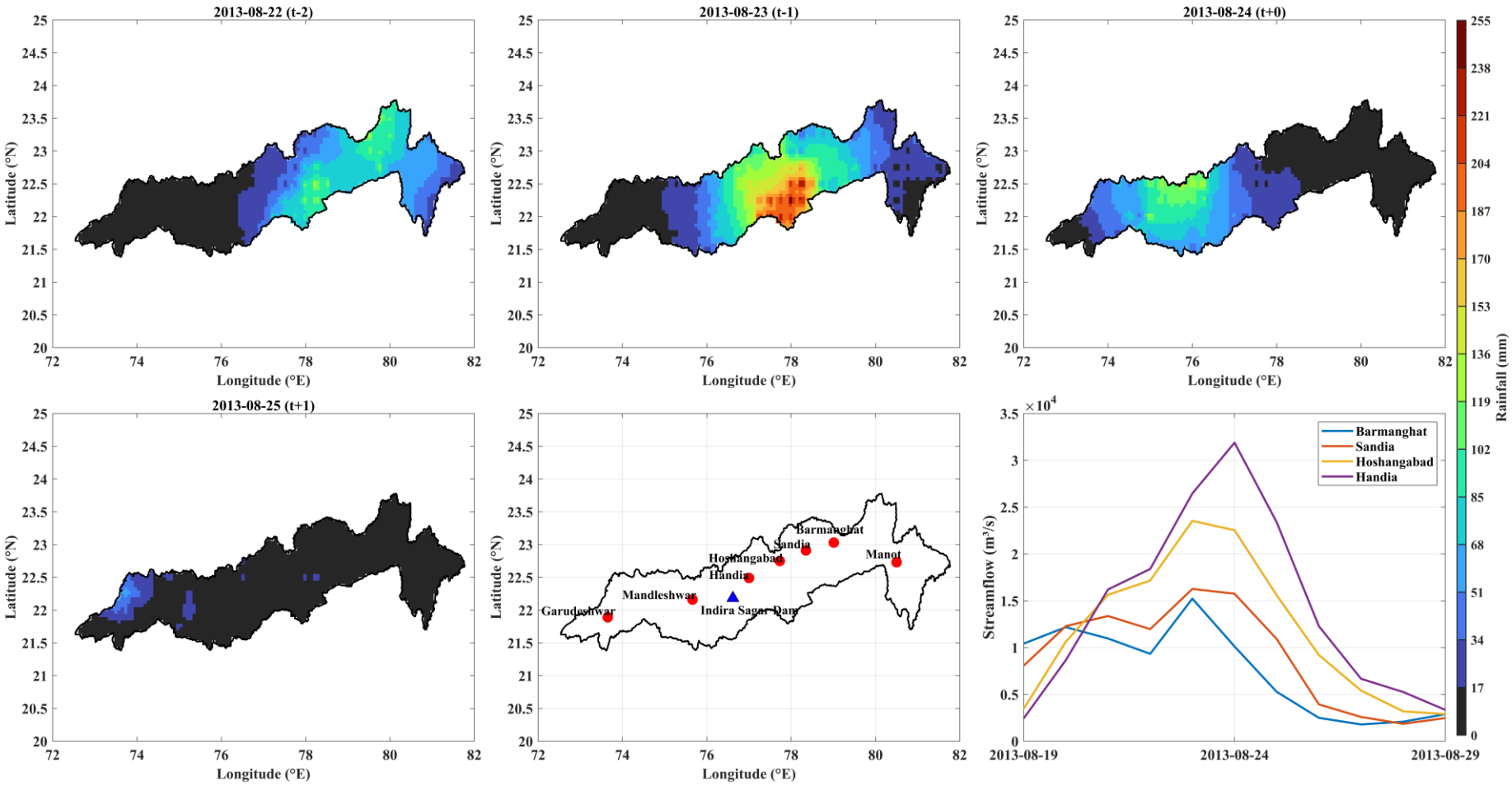

Figure 4.10 Spatial variability of daily rainfall, from day $(t-2)$ to $(t+1)$, across the Narmada River basin for the 2013 flood event and corresponding flood hydrograph for different stream gauges, where t represents the date of the peak flow.

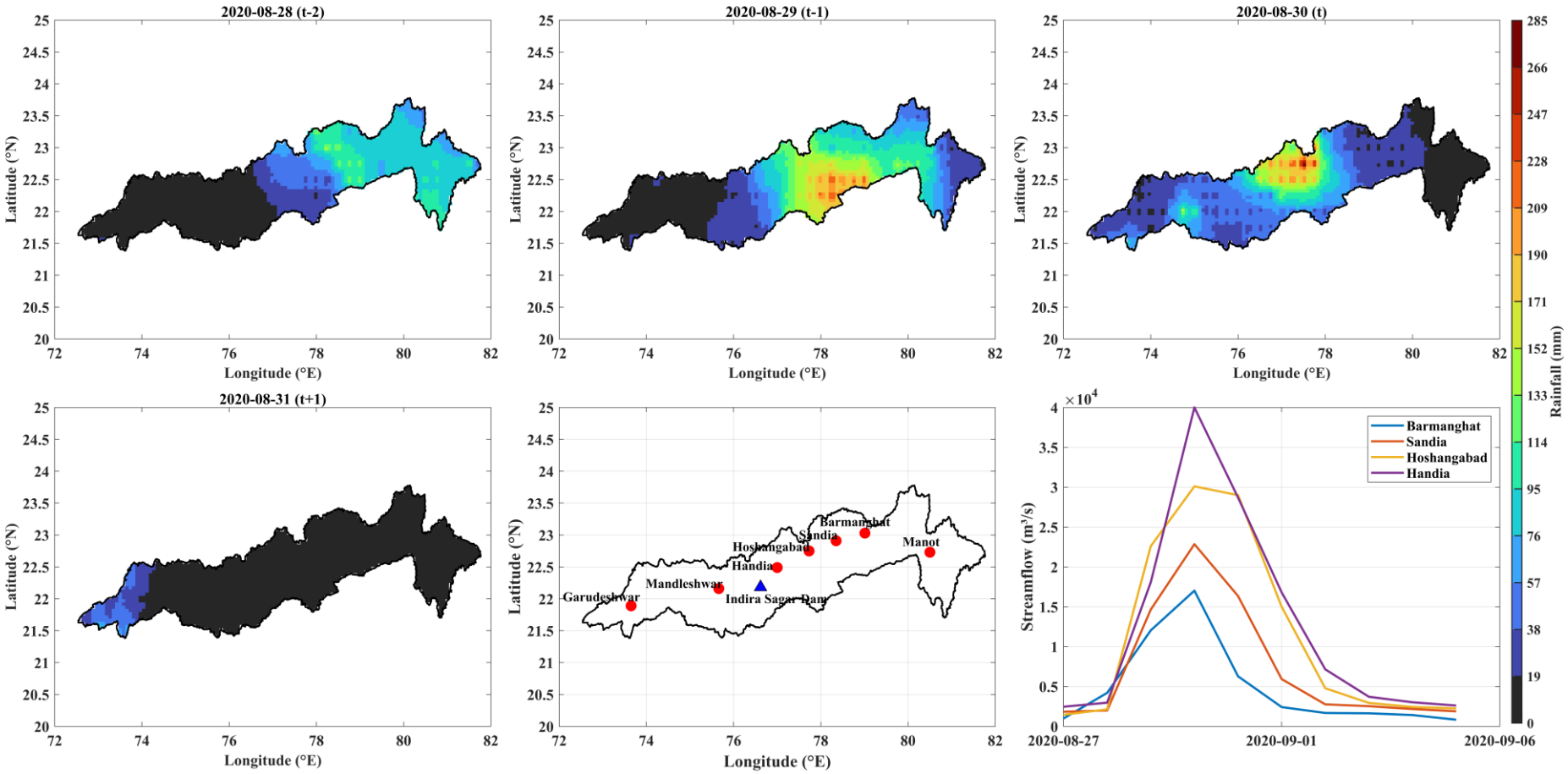

Figure 4.11 Spatial variability of daily rainfall, from day $(t-2)$ to $(t+1)$, across the Narmada River basin for the 2020 flood event and corresponding flood hydrograph for different stream gauges, where t represents the date of the peak flow.

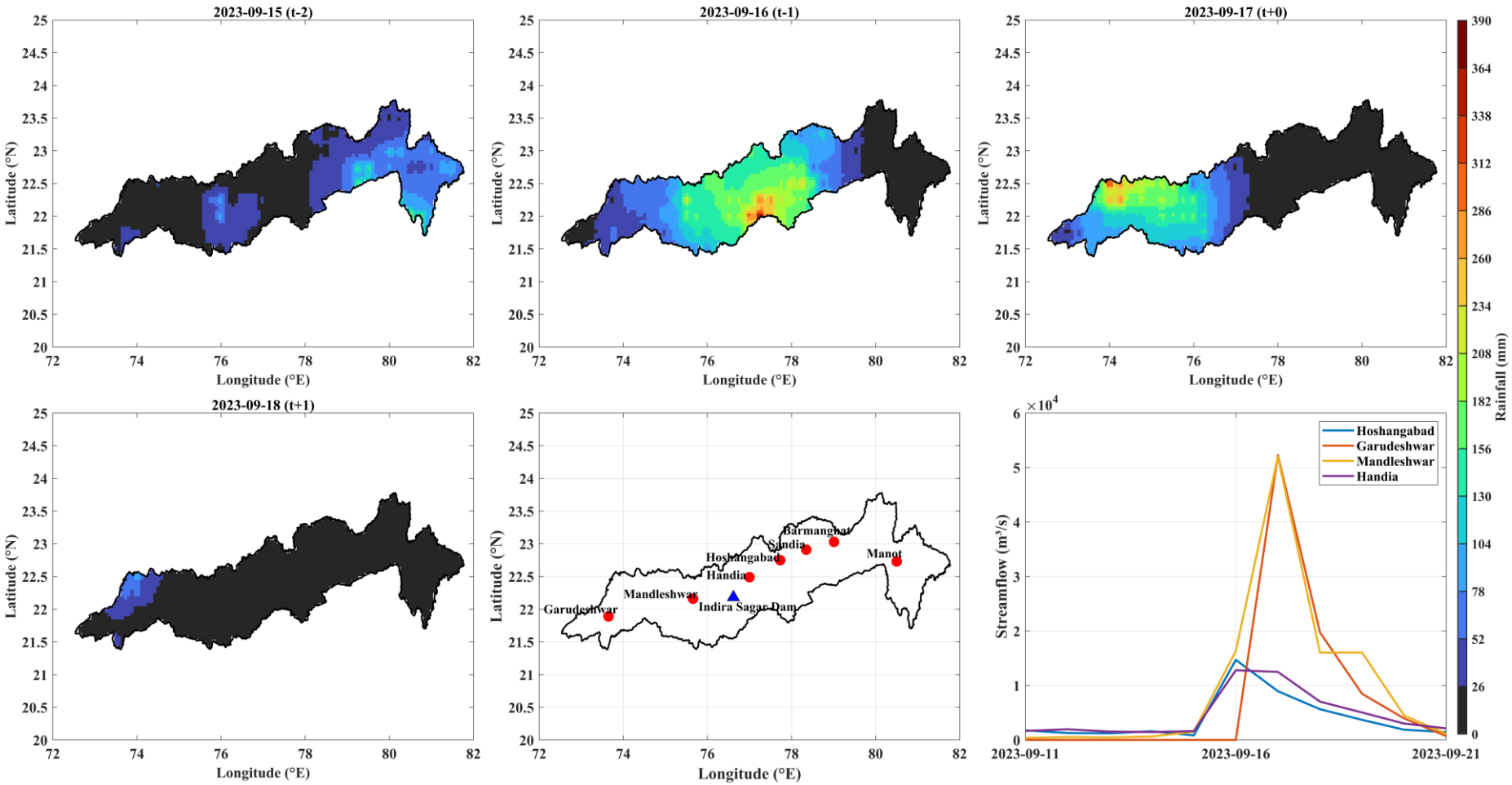

Figure 4.12 Spatial variability of daily rainfall, from day $(t-2)$ to $(t+1)$, across the Narmada River basin for the 2023 flood event and corresponding flood hydrograph for different stream gauges, where t represents the date of the peak flow.

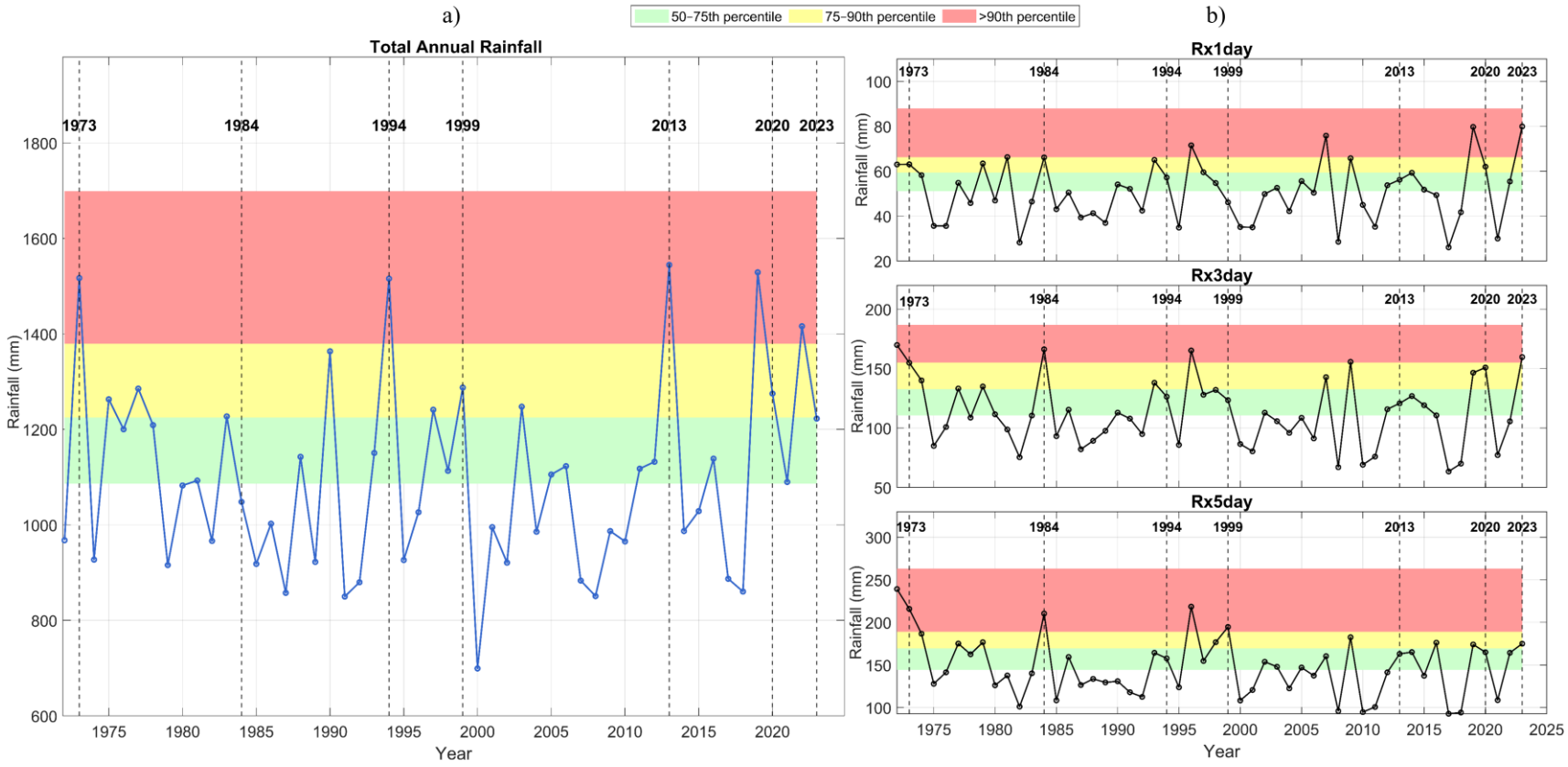

Figure 4.13 Temporal variation of (a) total annual rainfall and (b) Rx1day, Rx3day, and Rx5day for the selected flood events in the Narmada River basin, the dashed lines represent the years considered, red band represents values above 90th percentile, yellow band represents values between the 75th and 90th percentiles, and green band represents values between the 50th and 75th percentiles.

Reservoir level data for these events was obtained from the India-WRIS portal (https://indiawris.gov.in/wris/#/Reservoirs). Additionally, three extreme rainfall indices, viz., Rx1day, Rx3day, and Rx5day, representing one-day, consecutive three-day, and five-day maximum rainfall in a given year, were also estimated.

The 1973 flood event (see Figure 4.6) was marked by a classic upstream-to-downstream storm progression, with noticeable intensification near the Hoshangabad gauging station. This spatial movement of rainfall contributed to widespread flooding across the basin. A similar storm trajectory was observed in 1984 (see Figure 4.7), though the storm intensified more strongly over the upper-mid to mid-reaches of the basin. This resulted in localized peak rainfall intensities of 150–225 mm, triggering high flows at upstream stations like Hoshangabad and Handia. During both these floods no major reservoir was present, thus the accumulated runoff propagated downstream, leading to a peak discharge of approximately 50,000 cumecs at Garudeshwar.

The 1994 flood (see Figure 4.8) exhibited an upstream-to-downstream propagation pattern, but was notably intensified over the Chandwada catchment, where rainfall intensities reached 300–400 mm. This resulted in the highest ever peak flood recorded in the Orsang River at the Chandwada station, around 9,070 cumecs. Despite relatively low rainfall in the two days preceding the event, the flood magnitude was extraordinary, with Mandleshwar and Garudeshwar recording peak discharges of 48,200 and 60,642 cumecs, respectively. This can be attributed to the exceptionally high total monsoonal rainfall accumulated (June to September) across the basin approximately 1,400 mm, which is the highest recorded in the past 50 years. In comparison, the 1999 flood (see Figure 4.9) was more spatially confined, with rainfall primarily concentrated in the upstream regions. Although less extensive, it was characterized by high multi-day rainfall accumulation, resulting in localized but significant flooding at Barmanghat, Sandia, Hoshangabad, and Handia.

The 2013 flood (see Figure 4.10) showed peak rainfall intensities over the middle reaches of the basin. The presence of regulated reservoirs, filled to ~80% capacity helped moderate downstream impacts. Storm movement in this case remained consistent with the general upstream-to-downstream trend observed in other major events. The 2020 flood (see Figure 4.11) followed a similar pattern, with rainfall intensities of 200–300 mm focused on the upper and middle reaches. However, lower rainfall in downstream zones allowed for

relatively effective regulation, even though reservoirs were nearly 90% full prior to the event.

The most recent 2023 flood (see Figure 4.12) event was notable for very high localized rainfall intensities (250–400 mm) not only in the middle reaches but also extending to the lower reaches—a spatial distribution that compounded the severity of downstream flooding. With reservoirs already near their FRL, the system had limited buffering ability, resulting in Mandleshwar recording a peak discharge of record 52,000 cumecs, the highest ever recorded in its history.

From Figure 4.13, we can clearly categorize the flood events into three types based on the extreme rainfall indices and annual total rainfall: extreme precipitation-driven events, soil moisture or antecedent wetness-driven events, and those influenced by a combination of both mechanisms. The first category includes years such as 1984, which was primarily driven by extreme short-duration rainfall. This event recorded the highest Rx3day and second-highest Rx5day in the basin over the past five decades, while the annual rainfall was relatively low (less than 50^{th} percentile). The lack of significant antecedent wetness and the absence of major reservoir regulation suggests that this was a flood triggered almost entirely by an intense and short-lived precipitation burst.

The second category comprises events like 1994 and 2013, where flood severity was influenced more by sustained seasonal rainfall than by intense short-duration rainfall. In these years, Rx1day, Rx3day, and Rx5day values were moderate—mostly within the 50th to 75th percentile range—yet the basin experienced some of the highest annual rainfall totals. These wet antecedent conditions likely saturated the catchment, increasing runoff even under moderate storm conditions. Hence, these floods are best described as soil moisture-driven events.

The third category includes 1973, 1999, 2020, and 2023, which show characteristics of both intense short-duration rainfall and higher total annual rainfall, suggesting a combined influence of extreme precipitation and catchment wetness. In 1973, the basin recorded one of the highest annual rainfall along with high Rx3day and Rx5day values. The 1999 flood event, although spatially concentrated in the upper basin, featured Rx5day above the 90th percentile and reasonably high seasonal rainfall. The 2020 flood also had Rx3day and annual rainfall within the 75th to 90th percentile range. The 2023 flood event exhibited extremely high localized rainfall intensities, with the highest rainfall recorded in

a day in the past 50 years, and Rx3day and Rx5day above the 90th percentile, while also recording annual rainfall above the 90th percentile. This clearly positions 2023 among the events driven by a combination of extreme precipitation and pre-existing wet conditions, which is also one of the most severe flooding in recent years.

4.6. Role of Catchment Wetness

To understand the role of catchment wetness in driving floods, we selected the top 40 POT flood events for each catchment and calculated the Spearman rank correlation between flood magnitudes and the Antecedent Precipitation Buildup (APB) at different lags (lag 0 to lag 30). By analysing these correlations, we evaluated the influence of accumulated precipitation on flood magnitude across different catchments. From Figure 4.14, it is evident that catchments such as Barmanghat, Sandia, Hoshangabad, Chhidgaon, Handia, and Kogaon exhibit strong correlations between flood magnitudes and APB, indicating that catchment wetness plays a major role in flood generation in these regions. Catchments like Handia, Kogaon, and Chhidgaon show significant correlations extending to longer lags, suggesting that sustained wet conditions and excess soil moisture could be key drivers of higher flood magnitudes in these areas.

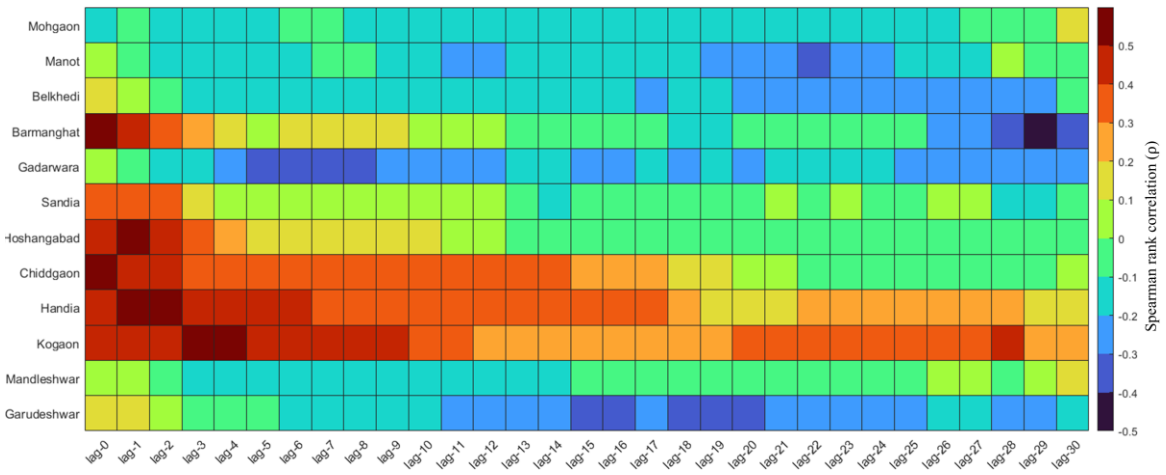

Figure 4.14 Dependence structure between peak-over-threshold (POT) flood magnitudes and antecedent precipitation buildup (APB) at various lags for the top forty POT events in each catchment. *The figure shows Spearman rank correlation (ρ) values between flood magnitudes and cumulative rainfall over d-day periods preceding the flood event, evaluated from lag 0 to lag 30 (x-axis), for each catchment (y-axis). Higher correlation values indicate stronger influence of antecedent rainfall on flood magnitude, highlighting the role of catchment wetness in flood generation.*

In contrast, flood magnitudes at catchments such as Mohgaon, Manot, Belkhedi, Gadarwara, Mandleshwar, and Garudeshwar show weak or no significant correlation with

APB. This implies that antecedent rainfall buildup may have limited influence on the magnitude of floods in these catchments, and that such floods are more likely triggered by short-duration extreme precipitation events or a combination of both extreme rainfall and catchment wetness. Notably, Mandleshwar and Garudeshwar on the Narmada River are regulated by the Indira Sagar and Sardar Sarovar reservoirs, respectively. These stations along the mainstream river display relatively low correlation with APB, highlighting the dominant role of reservoir operations in modulating flood magnitudes at these stations.

4.7. Closure

The results and discussions in this chapter provide a comprehensive understanding of the temporal and spatial dynamics of floods in the Narmada basin. The integration of statistical analyses with hydro-meteorological insights offers a nuanced perspective on flood behaviour and its driving factors. These findings form the basis for the conclusions and recommendations presented in the final chapter of the study.

Chapter - 5

CONCLUSIONS AND FUTURE SCOPE

5.1. Key Conclusions

This study provides valuable insights into flood dynamics in the Narmada River basin through a comprehensive analysis of flood timings, magnitudes, and their trends. Our findings reveal significant patterns that underscore the importance of adaptive management strategies to address the evolving nature of flooding in the region. The key findings are:

(i) The analysis reveals that the mean flood timing in the Narmada basin is mid-August (using both AMS and POT approaches), with the Kundi River exhibiting the widest range of flood occurrence timings, highlighting variability in flood timings.

(ii) The severe most flood in the Narmada basin was observed at the Garudeshwar station in 1994 of magnitude 60642 cumecs, with an estimated return period of 47 years using the AMS approach and 98 years using the POT approach. The AMS series shows a high percentage of large floods at the Barmanghat, Chiddgaon, and Manot stations, while at Belkhedi and Handia stations using POT approach. Furthermore, the POT series had a lower percentage of large floods, but a higher percentage of medium floods compared to AMS.

(iii) A declining trend in flood magnitude is observed in the AMS series, particularly at mainstream stations like Barmanghat, Hoshangabad, Mandleshwar, and Garudeshwar, and tributary stations such as Mohgaon, Belkhedi, and Gadarwara. The POT series also shows decreasing trends at several stations, though catchments like Handia, Sandia, and Manot exhibit increasing trends. A significant decline in streamflow is observed in Hoshangabad in both the AMS and POT approaches.

(iv) The AMS series shows no significant trends in flood timing, while increasing trend is visible at most mainstream stations. The POT series highlights a significant delay in peak flood timing at Mohgaon, Sandia, and Garudeshwar, with most other stations also showing an increasing trend in flood timing, except Belkhedi and Gadarwara.

(v) Based on the flood analysis, three typologies of flood events were identified: (i) extreme precipitation-driven events, such as the 1984 flood, characterized by intense short-duration rainfall and low seasonal accumulation, indicating limited influence of antecedent wetness; (ii) soil moisture-driven events, like those in 1994 and 2013,

where moderate short-duration rainfall combined with exceptionally high seasonal rainfall suggests catchment saturation played a dominant role; and (iii) combination events, including 1973, 1999, 2020, and 2023, where both high rainfall intensities and elevated annual rainfall contributed, highlighting the joint influence of extreme precipitation and antecedent wetness in amplifying flood severity.

(vi) Catchment-wise correlation analysis between flood magnitudes and antecedent precipitation buildup reveals a clear spatial distinction in flood-generating mechanisms across the Narmada basin. In the upper and middle catchments—such as Barmanghat, Sandia, Handia, and Hoshangabad—flood magnitudes are strongly influenced by catchment wetness, with significant correlations observed even at longer lags. This highlights the role of sustained precipitation and soil moisture accumulation in amplifying flood responses. In contrast, stations like Mandleshwar and Garudeshwar, which are regulated by major reservoirs such as Indira Sagar and Sardar Sarovar, exhibit weak or no correlation with antecedent precipitation, suggesting that flood magnitudes in these regions might be controlled by other factors such as reservoir operations, regulated releases, or localised extreme rainfall events.

5.2. Future Scope of study

This study provides a foundational understanding of flood-generating mechanisms in the Narmada River basin, with emphasis on the roles of extreme precipitation events and antecedent precipitation buildup. Building upon this, future research will incorporate satellite-derived or modeled soil moisture data to directly examine the relationship between flood magnitudes and antecedent soil moisture conditions. This will allow for a more explicit attribution of floods to wet catchment conditions, extreme rainfall, or their combined influence, thereby facilitating a deeper catchment-level understanding of flood drivers and supporting more targeted flood management strategies. Additionally, future work will focus on identifying the maximum fortnightly probability of flood occurrence for each catchment. This will involve determining the specific fortnightly window during which floods are most likely to occur, using either empirical distributions or parametric distribution fitting. Such analysis will provide critical information for improving the timing of flood preparedness measures and optimizing resource allocation during the flood season. These future directions will enhance the understanding of flood dynamics and contribute to the development of more effective flood mitigation and management strategies.

REFERENCES

Bhargav, A. M., Suresh, R., Tiwari, M. K., Trambadia, N. K., Chandra, R., and Nirala, S. K. (2025). Development of a 2D hydrodynamic model for flood assessment for the lower Narmada basin, Gujarat (India). *Journal of Water and Climate Change*, 16(4), 1567-1585.

Burn, D. H., Whitfield, P. H., and Sharif, M. (2016). Identification of changes in floods and flood regimes in Canada using a peaks over threshold approach. *Hydrological Processes*, 30(18), 3303-3314.

Cunnane, C. (1979). A note on the Poisson assumption in partial duration series models. *Water Resources Research*, 15(2), 489-494.

CWC (2014). *Narmada Basin Report*, Central Water Commission, New Delhi.

Do, H. X., Westra, S., Leonard, M., and Gudmundsson, L. (2020). Global-scale prediction of flood timing using atmospheric reanalysis. *Water Resources Research*, 56(1), e2019WR024945.

Ganguli, P., Nandamuri, Y. R., and Chatterjee, C. (2023). Understanding flood regime changes of the Mahanadi River. *ISH Journal of Hydraulic Engineering*, 29(3), 389-402.

Hamed, K. H., and Rao, A. R. (1998). A modified Mann-Kendall trend test for autocorrelated data. *Journal of Hydrology*, 204(1-4), 182-196.

Hunt, K. M., and Fletcher, J. K. (2019). The relationship between Indian monsoon rainfall and low-pressure systems. *Climate Dynamics*, 53(3), 1859-1871.

Jain, S. K., Agarwal, P. K., Singh, V. P., Jain, S. K., Agarwal, P. K., and Singh, V. P. (2007). Narmada basin. In *Hydrology and Water Resources of India*, 513-559.

Jain, S. K., Nayak, P. C., Singh, Y., and Chandniha, S. K. (2017). Trends in rainfall and peak flows for some river basins in India. *Current Science*, 1712-1726.

Kale, V. S. (2003). Geomorphic effects of monsoon floods on Indian rivers. In *Flood Problem and Management in South Asia*, 65-84.

Kale, V. S., Hire, P., and Baker, V. R. (1997). Flood hydrology and geomorphology of monsoon-dominated rivers: the Indian Peninsula. *Water International*, 22(4), 259-265.

Kale, V. S., Mishra, S., and Baker, V. R. (2003). Sedimentary records of palaeofloods in the bedrock gorges of the Tapi and Narmada rivers, central India. *Current Science*, 1072-1079.

Kathal, P. K. (2018). Narmada: the longest westward flowing river of the peninsular India. *The Indian Rivers: Scientific and Socio-economic Aspects*, 301-308.

Kendall, M. G. (1975). Rank Correlation Methods. *Charles Griffin, London*.

Langbein, W. B. (1949). Annual floods and the partial-duration flood series. *Eos, Transactions American Geophysical Union*, 30(6), 879-881.

Lehmann, E. L. (1975). Statistical methods based on ranks. *Nonparametrics. San Francisco, CA, Holden-Day*, *2*.

Mangini, W., Viglione, A., Hall, J., Hundecha, Y., Ceola, S., Montanari, A., Rogger, M., Salinas, J.L., Borzì, I. and Parajka, J. (2018). Detection of trends in magnitude and frequency of flood peaks across Europe. *Hydrological Sciences Journal*, 63(4), 493-512.

Mangukiya, N. K., Mehta, D. J., and Jariwala, R. (2022). Flood frequency analysis and inundation mapping for lower Narmada basin, India. *Water Practice & Technology*, 17(2), 612-622.

Mann, H. B. (1945). Nonparametric tests against trend. *Econometrica: Journal of the Econometric Society*, 245-259.

Mazas, F. (2019). Extreme events: a framework for assessing natural hazards. *Natural Hazards*, 98(3), 823-848.

Mostofi Zadeh, S., Durocher, M., Burn, D. H., and Ashkar, F. (2019). Pooled flood frequency analysis: a comparison based on peaks-over-threshold and annual maximum series. *Hydrological Sciences Journal*, 64(2), 121-136.

Nanditha, J. S., Rajagopalan, B., and Mishra, V. (2022). Combined signatures of atmospheric drivers, soil moisture, and moisture source on floods in Narmada River basin, India. *Climate Dynamics*, 59(9), 2831-2851.

National Disaster Management Guidelines. Management of Floods, <https://ndma.gov.in/sites/default/files/PDF/Guidelines/flood.pdf>.

Pandey, B. K., and Khare, D. (2018). Identification of trend in long term precipitation and reference evapotranspiration over Narmada river basin (India). *Global and Planetary Change*, 161, 172-182.

Petrow, T., and Merz, B. (2009). Trends in flood magnitude, frequency and seasonality in Germany in the period 1951–2002. *Journal of Hydrology*, 371(1-4), 129-141.

Rajaguru, S. N., Gupta, A., Kale, V. S., Mishra, S., Ganjoo, R. K., Ely, L. L., Enzel, Y., and Baker, V. R. (1995). Channel form and processes of the flood-dominated Narmada River, India. *Earth Surface Processes and Landforms*, 20, 407–421.

Ray, L. K., and Goel, N. K. (2019). Flood frequency analysis of Narmada river basin in India under nonstationary condition. *Journal of Hydrologic Engineering*, 24(8), 05019018.

Roxy, M. K., Ritika, K., Terray, P., Murtugudde, R., Ashok, K., and Goswami, B. N. (2015). Drying of Indian subcontinent by rapid Indian Ocean warming and a weakening land-sea thermal gradient. *Nature Communications*, 6(1), 7423.

SDMA (2020). *State Disaster Management Authority*, Government of Madhya Pradesh. Paryavaran Parisar, Bhopal, MP.

Singh, S., Kumar, N., Goyal, M. K., and Jha, S. (2023). Relative influence of ENSO, IOD, and AMO over spatiotemporal variability of hydroclimatic extremes in Narmada basin, India. *AQUA—Water Infrastructure, Ecosystems and Society*, 72(4), 520-539.

Subramanya, K., and Sharma, P. J. (2024). *Engineering Hydrology* (6th Ed.), McGraw Hill Publications, New Delhi.

Waikhom, S. I., Yadav, V. K., Chadee, A. A., and Varma, V. (2023). Variability in trends of streamflow and precipitation in the Narmada River Basin over the past four decades. *Water Supply*, 23(3), 1495-1518.

Williams, G. P. (1978). Bank-full discharge of rivers. *Water Resources Research*, 14(6), 1141-1154.

Zhang, Q., Zhang, L., She, D., Wang, S., Wang, G., and Zeng, S. (2021). Automatic procedure for selecting flood events and identifying flood characteristics from daily streamflow data. *Environmental Modelling and Software*, 145, 105180.